Magnetite Oxidation in Aqueous Systems

John A. Templeton

Thesis submitted to the faculty of The Virginia Polytechnic and State University in partial fulfillment of the requirements for the degree of

Masters of Science
in
Environmental Engineering

Peter J. Vikesland, Ph.D., Chair
Andrea M. Dietrich, Ph.D
Marc A. Edwards, Ph.D

June 18 2008
Blacksburg, Virginia

Keywords: Magnetite, maghemite, oxidation, UV-VIS-NIR, spectroscopy, transition

Magnetite Oxidation in Aqueous Systems

John Templeton

Abstract

Magnetite, an iron oxide, is a possible candidate for *in situ* remediation of contaminated groundwater systems due to its oxidation/reduction potential for reduction of contaminants such as carbon tetrachloride. Little characterization and analysis has been done to describe the kinetics of magnetite transformation during oxidation. This work focuses on monitoring the concentrations of magnetite and one of its oxidation transformation products, maghemite, by the use of UV-Vis-NIR spectroscopy. As oxidation proceeded at a constant specific temperature, the concentration of magnetite decreases, which was indicated by a decrease in absorption in the NIR-region of the spectrum. As magnetite concentrations decreased, the concentration of maghemite increased, which was indicated by an increase in absorption in the UV-region. The temperature at which the suspensions of magnetite and maghemite were measured was of great importance for complete understanding of the magnetite transformation as seen by UV-Vis-NIR spectroscopy analysis. Higher measurement temperatures produced higher absorptivities of Fe^{II}-Fe^{III} electron hopping transitions, while decreasing the absorptivity of Fe^{III}-Fe^{III} in the NIR and UV-regions respectively. Lower temperatures produced the opposite effects on the iron oxides' transitions. Higher temperature increased the rate of oxidation.

Acknowledgements

I would like to acknowledge the leadership and assistance of my advisor, Dr. Peter Vikesland. Despite his heavy work load with classes and a large research group, he was always very accessible and helpful. I would also like to mention the help I received from my other committee members, Dr. Andrea Dietrich, and Dr. Marc Edwards. Both were professors of mine in aquatic chemistry which greatly aided my understanding the aspects of my research. Robert Rebodos, a member of my research group, was an unparalleled friend and mentor who made every effort to help me obtain my goals. My research was funded by LUNA Innovations Inc. to whom I am very grateful.

I have enjoyed my time as a student here in the Civil and Environmental Department at Virginia Tech. The friends I have made and the experiences and knowledge that I have gained from working with both faculty and students will never be forgotten or matched as I development my professional career. I had the privilege of working with an outstanding research group that was always a source of support. Special thanks are owed to Julie Petruska, Jodie Smiley, Charles Farley, Betty Wingate, and Beth Lucas for their constant assistance in and out of the lab.

Finally, I would like to thank my friends and family. I have been blessed with an amazing family; Reed, Elizabeth, and Laura Templeton, who made everything I have achieved possible through their love and support in everything that I have done.

Table of Contents

Table of Tables

Table of Figures

I. Introduction

Background

Iron oxides are found worldwide and have proven to be useful to humans since the beginning of civilization [1]. The iron and oxygen compounds have been of increasing importance as the knowledge of their structures and reactivity has developed [2]. The properties of iron oxides are dependent on the arrangement of the iron and oxygen atoms within the crystalline structure. Magnetite is a composite of divalent iron (Fe^{II}) and trivalent iron (Fe^{III}) that is found naturally but is also a major corrosion product of some iron based drinking water systems [3]. The mixture of oxidation states of iron present unique characteristics for magnetite such as their adsorption of certain contaminants, such as arsenic, and their reactivity with chlorinated hydrocarbons [2, 4, 5].

Magnetite is not a stable iron oxide. At increased temperatures and exposure to oxidants, magnetite can be readily oxidized to maghemite. At extremely high temperatures, magnetite can be further oxidized to hematite [6]. As stated earlier, magnetite is a composite of both oxidation states of iron. Through the process of oxidation, the Fe^{II} diffuses from within the magnetite structure and oxidizes at the surface, donating an electron to an oxidant, becoming Fe^{III}. When maghemite is the oxidation product, the transformation is referred to as a topotactic transformation, since the crystalline structure remains constant; however, containing only Fe^{III}. Under further oxidation to hematite, the structure changes from close cubic packed to hexagonal close packed, which describes how the oxygen anions within the structure are arranged. These transformations of magnetite result in an alteration of properties and characteristics.

Numerous studies have identified magnetite and maghemite as well as many other iron oxides by the use of spectroscopy and diffraction [1, 6]. Diffraction methods, such as X-ray diffraction, are limited by the fact that the crystalline structure of maghemite and magnetite are the same [1]. The use of Raman spectroscopy has proven effective for identifying the different iron oxides; however, little has been done to monitor the transformation process of one iron oxide to another by Raman spectroscopy analysis [6].

UV-Vis-NIR spectroscopy can monitor the change in magnetite to maghemite through changing absorptions within the electromagnetic spectrum [5]. Absorption bands appear throughout the spectrum due to different transitions that arise from excitations produced by the spectrometer within the sample. In the UV-region of the spectrum, iron oxides present a Fe^{III}-Fe^{III} transition with an intense absorption peak [7]. Within the NIR-region, there is a charge transfer transition, involving Fe^{II} to Fe^{III} electron hopping [8]. There are few studies that have monitored the change in magnetite concentrations through changing UV-Vis-NIR absorption as most oxidation kinetics are done according to Fe^{II} concentration changes [5, 9]. There has yet to have been extensive work on the changing maghemite concentrations in conjunction with changing magnetite concentrations using any form of spectroscopy.

Research Objectives

Identification of iron oxides by the use of spectroscopy and diffraction is well established. The oxidation process of magnetite has been investigated extensively. Combining these two aspects of iron oxide analysis has proven to be a challenge. It is the overall goal of this study to monitor the oxidation of magnetite through changes in

identifying absorption bands of UV-Vis-NIR spectroscopy. The following list of goals facilitated the overall goal of the research.

1) To produce nanoscale pure magnetite particles.
2) To establish a method of controlled oxidation of magnetite.
3) To evaluate the effect of various temperatures on the oxidation kinetics of magnetite by analyzing the changing absorption bands within the UV-Vis-NIR spectrum.
4) To reach a better understanding of the interactions between the UV-Vis-NIR light source, measurement temperature, and the sample transitions.

Thesis Outline

The thesis is presented in six chapters; this introductory chapter being the first. Chapter II provides background information for iron oxides and magnetite. Within the chapter, information will be found characterizing iron oxides and magnetite, preparation/formation, transformation, surface properties, as well as remediation capabilities. Chapter III explains the oxidation process and use of the UV-Vis-NIR spectrometer. Specific iron oxide transitions are explained, which cause the different absorptions within the spectrum. Chapter III concludes by analyzing the effect of temperature on the oxidation kinetics of magnetite. Chapter IV presents the preliminary work done for oxidation using Raman spectroscopy, dynamic light scattering, and arsenic adsorption. Chapter V discusses the engineering significance of the study, and the final chapter, Chapter VI, states the conclusions drawn from the study.

References

1. R.M. Cornell, U.S., *The Iron Oxides Structure, Properties, Reactions, Occurrences and Uses*. Second ed. 2003: Wiley-VCH Verlag GmbH & Co. KGaA, Weinheim. 664.
2. McCormick, M.L., E.J. Bouwer, and P. Adriaens, *Carbon tetrachloride transformation in a model iron-reducing culture: Relative kinetics of biotic and abiotic reactions.* Environmental Science & Technology, 2002. 36(3): p. 403-410.
3. Zhang, Z., et al., *Effect of pipe corrosion scales on chlorine dioxide consumption in drinking water distribution systems.* Water Research, 2008. 42(1-2): p. 129-136.
4. Vikesland, P.J., et al., *Particle size and aggregation effects on magnetite reactivity toward carbon tetrachloride.* Environmental Science & Technology, 2007. 41(15): p. 5277-5283.
5. Tang, J., et al., *Magnetite Fe3O4 nanocrystals: Spectroscopic observation of aqueous oxidation kinetics.* Journal of Physical Chemistry B, 2003. 107(30): p. 7501-7506.
6. Shebanova, O.N. and P. Lazor, *Raman study of magnetite (Fe3O4): laser-induced thermal effects and oxidation.* Journal of Raman Spectroscopy, 2003. 34(11): p. 845-852.
7. Sherman, D.M. and T.D. Waite, *Electronic-Spectra of Fe-3+ Oxides and Oxide Hydroxides in the near Ir to near Uv.* American Mineralogist, 1985. 70(11-12): p. 1262-1269.
8. Fontijn, W.F.J., et al., *A consistent interpretation of the magneto-optical spectra of spinel type ferrites (invited).* Journal of Applied Physics, 1999. 85(8): p. 5100-5105.
9. Sidhu, P.S., R.J. Gilkes, and A.M. Posner, *Mechanism of Low-Temperature Oxidation of Synthetic Magnetites.* Journal of Inorganic & Nuclear Chemistry, 1977. 39(11): p. 1953-1958.

II. Literature Review

Iron Oxides

Iron oxides, consisting of varying ratios of iron and oxygen, are commonly found in nature. The weathering of iron bearing rocks accompanied by mechanical transportation, distributes iron throughout the earth's biosphere, lithosphere, pedosphere, hydrosphere, and atmosphere. Most iron oxides contain only the trivalent form of iron (Fe^{III}), however, there are some that contain both trivalent and divalent iron (Fe^{II}). The magnetic properties of many rocks can be partially attributed to the iron oxide, magnetite, Fe_3O_4, which contains both Fe^{II} and Fe^{III}. γ-Fe_2O_3, maghemite, is a red-brown weathering product of magnetite and other iron oxides. α-Fe_2O_3, hematite, is the end product of many iron oxide transformations including that of magnetite.

The chemical compositions and structures of iron oxides dictate their specific properties and their ultimate use. One of the oldest and simplest uses of iron oxides has been as a coloring agent for artistry. Prehistoric rock paintings were produced from iron oxides and as time progressed the development of pigments from iron oxides helped create ceramics and pottery. Technological developments have diversified the uses of iron oxides. Investigating the magnetic properties of some iron oxides has aided in the advancement of navigation as well as ferrofluids. Ferrofluids are a suspension of nanoscale magnetic iron oxide particles, such as magnetite, which respond to external magnetic forces. Ferrofluids have been used widely in engineering for products such as liquid seals around spinning drive shafts of computer hard drives to keep debris out of the computer system. Due to their friction reducing capabilities, ferrofluids are also used as lubricants in machinery. Aside from their magnetic properties, iron oxides have various

other practical uses. Hematite is used as a catalyst in airbags, and magnetite is used in coal washing due to its low cost, hardness, and chemical stability. Possible medicinal uses are being investigated for many iron oxides [1]. Environmental remediation is an area of rising interest for iron oxides as some iron oxides have shown adsorption and reductive capabilities [2, 3]. Iron oxides form very small particles with high surface areas ($m^2\ g^{-1}$), which may increase the adsorption and reductive capabilities of the particles [4, 5].

Iron Oxide Characterization

Iron oxide identity depends on the configuration of iron (Fe) and oxygen (O) in a crystal lattice. Of the 16 most common iron oxides, only three are discussed herein: magnetite and its two oxidation products maghemite and hematite. Magnetite is a composite of divalent (Fe^{II}) and trivalent (Fe^{III}) iron ($Fe^{II}Fe_2{}^{III}O_4$) and is commonly found in beach sand and the course, heavy mineral fraction of soils of all parts of the world. Maghemite has the same structure as magnetite, cubic close packed (ccp); however, maghemite has iron deficiencies and contains no divalent iron. Solid solutions of magnetite/maghemite are common. Hematite contains no divalent iron and its' hexagonal close packed (hcp) structure differs greatly from than that of magnetite and maghemite. [6]. Figure 2-1 illustrates the crystalline structures of these three iron oxides. A ccp crystal has three sheets of anions, each positioned differently and stacked as ABCABC; each letter representing a different sheet arrangement. An hcp crystal has only two sheets of anions with different positions and stacked as ABAB. The spaces left by the anions are filled by iron cations or sometimes remain vacant as in maghemite and hematite.

Diffraction

X-ray diffraction (XRD) is a type of diffractometry that measures the interaction between X-rays and a solid. XRD is able to determine the regular and long-range atomic configurations of a crystal. The X-ray wavelength used is approximately 0.1 nm. This wavelength is comparable to the distance between atoms in a crystal. When X-rays interact with the atoms they diffract at different angles, thus describing the crystalline structure. Because maghemite and magnetite have the same ccp crystal structure, their diffractograms are identical. When these iron oxides further oxidize to hematite, the structure changes from ccp to hcp, resulting in a different diffractogram. Figure 2-2 presents the XRD diffractograms for magnetite, maghemite, and hematite. Cubic close packed and hexagonal close packed refers to the arrangement of the anions in the structure.

Spectroscopy

Spectroscopic techniques commonly used to identify iron oxides include infrared (IR), ultraviolet-visible (UV-VIS), and Raman spectroscopy [7].

Infrared spectroscopy. Electromagnetic radiation from 1-300 μm will be absorbed differently by molecules depending on their rotational energy levels and the force constants of the interatomic bonds [6]. This information is used to identify the iron oxide, provide information about crystal morphology, degree of crystallinity, as well as information about adsorbed molecules and surface complexes of the iron oxide. Figure 2-3 presents the infrared spectroscopy data for the three iron oxides.

Raman spectroscopy. Raman spectroscopy measures the electromagnetic scattering of a molecule caused by the illumination of a laser of a specific wavelength in

the ultraviolet and visible regions. The laser that is used in Raman spectroscopy has a specific wavelength/energy. As the laser is shone on the sample, the molecules scatter most of the energy at the same wavelength as the laser; however, some of the energy is scattered below or above the laser wavelength. The energy differences are quantified in terms of Raman shifts that correspond to chemical bonds in the sample. Each iron oxide produces several Raman shifts that are representative of that specific iron oxide. Lasers may cause an increase in sample's temperature leading to a possible false measurements due to a change in the sample itself [8]. In the case of iron oxides, oxidation induced by the laser is possible; therefore, care must be taken when using Raman spectroscopy [8].

UV-Vis-NIR spectroscopy. UV-Vis-NIR spectroscopy uses light to excite the valence electrons of a molecule. Different wavelengths of light are comprised of specific degrees of energy that cause different electron transitions. Therefore, the structure and composition of an iron oxide will dictate its electron configurations and possible transitions that the spectrometer may excite. UV-VIS-NIR spectroscopy measures three characteristics of an iron oxide solid. The first is trivalent iron crystal or ligand field transitions. The second is the interaction of magnetically coupled trivalent iron and the third is ligand (oxygen)-metal charge transfer excitations from the O(2p) non-bonding valence bands to the Fe(3d) ligand field orbitals or possibly between Fe^{II} and Fe^{III} [6]. The temperature at which the sample is measured alters the compounds molar absorptivity. Molar absorptivity is the degree to which light at a specific wavelength can be absorbed. These properties are related through Beer's Law.

$$\text{Beer's Law} = \text{Absorbance} = \varepsilon bc \quad \text{(Equation 1)}$$

Where ε = molar absorptivity
b = path length

c = concentration

The UV-Vis-NIR spectra for these iron oxides can be seen in Figure 2-4.

Magnetite

Nanoparticle iron oxides are of interest to the environmental engineering field due to their properties and affinity for certain compounds [6]. Powdered magnetite is currently used to adsorb cations in sewage treatment [6]. Ferrofluids containing magnetite are being explored for their possible use in bioscience, computer science, and medicine. The magnetic properties of magnetite lend its possible use to magnetic recordings, high performance electromagnetic and spintronic devices, and *in situ* environmental remediation [9, 10].

Formation/Synthesis

Magnetite can be formed by a multitude of ways. In laboratory settings magnetite is readily synthesized by the co-precipitation of Fe^{II} and Fe^{III} in alkaline media. The size of the particles is dependent on the pH and the ionic strength of the system. Smaller particles result from high ionic strength and high pH systems [10]. Other laboratory methods involve the hydrolysis of Fe^{II} to green rust, which then can be oxidized to magnetite [11]. Corrosion of zero-valent iron and the reduction of hematite at high temperatures result in magnetite [6]. Permeable reactive barriers that corrode may develop magnetite on the iron surface [12]. The use of chlorine dioxide as a disinfectant has been shown to cause corrosion in iron piping of drinking water systems. One of the major corrosion products of this nature is magnetite [13]. Magnetite is naturally found in soils and sands throughout the world. Intracellular magnetite production by the reduction of Fe^{III} within magnetosomes of some bacteria is being investigated [14].

Characterization

Most iron oxides contain only trivalent iron (Fe^{III}); however, some contain divalent iron (Fe^{II}) as well. The oxygen atoms of iron oxides typically take a hexagonal close packed (hcp) or cubic close packed (ccp) configuration. The trivalent and divalent iron fill the interstices, commonly in the tetrahedral or octahedral co-ordinations. The energy of crystallization for iron oxides is quite high, leaning towards formation of small crystals with high surface areas per unit mass. Different structures and configurations distinguish different iron oxides [6].

X-ray diffraction (Figure 2-3) has shown that magnetite has an inverse spinel configuration with a face-centered cubic (fcc) unit cell based on 32 oxygen anions (Figure 1-1). The formal structure for magnetite is written as $Fe^{III}[Fe^{II}Fe^{III}]O_4$, where the brackets indicate octahedral sites, showing that trivalent iron is present in both octahedral and tetrahedral sites, while Fe^{II} is confined to octahedral sites. Stoichiometric magnetite has twice as much trivalent iron as divalent iron [6]. Magnetite is an inverse spinel because the tetrahedral sites are occupied by trivalent iron, while in a normal spinel the tetrahedral sites are occupied by the divalent form of the metal [15]. At room temperature, magnetite is ferromagnetic due to the presence of two interpenetrating magnetic sublattices. These lattices have antiparallel, unequal spin magnitudes and this causes magnetite to be ferrimagnetic [6].

Raman spectroscopy can be used to distinguish between magnetite and its oxidation products. Magnetite has a strong Raman band at 667 cm^{-1}. The strongest bands for maghemite are present at 381, 670, and 781 cm^{-1}. Hematite is identified by

bands at 226 and 292 cm^{-1}. These iron oxides may have additional defining peaks, however, they typically have lower intensities.

UV-Vis-NIR spectra exhibit high absorption in the UV-VIS region for red and yellow iron oxides and low absorption in the NIR-region for maghemite and hematite. Magnetite has a maximum absorption in the NIR-region around 1500 nm due to electron hopping between Fe^{II} and Fe^{III} in the octahedral sites. Stoichiometric maghemite and hematite contain no Fe^{II}; therefore, the oxidation products of magnetite do not absorb in the NIR-region.

Monitoring the transformation of magnetite to maghemite and hematite is experimentally challenging. Irradiation by the Raman laser can cause particle oxidation, and the XRD diffractions are the same for magnetite and maghemite [8]. UV-Vis-NIR, however, shows promising differences between magnetite and maghemite [16]. In the NIR-region, the strong absorption of magnetite decreases as the sample changes from magnetite to maghemite, as maghemite does not absorb in this wavelength range [16]. The band monitored throughout oxidation is a intervalence charge transfer (IVCT) adsorption band present in the NIR-region [16]. Figure 6 shows the reduction of adsorption in the NIR-region that occurs as oxidation proceeds [16].

Transformations

Chemical transformations of iron oxides can occur via dehydration, dehydroxylation, or oxidation/reduction reactions. A structural change can either be topotactic or reconstructive. Topotactic changes occur within a single crystal of the solid phase, producing a product with the same three dimensional configuration as its predecessor. Topotactic transformations usually take place at higher temperatures which

aid in mobility within the crystal. Reconstructive transformations occur when the entire iron oxide is dissolved and then reforms as a new structure [6].

Oxidation. The oxidation of magnetite initially occurs as a chemical, topotactic transformation to maghemite, but ultimately becomes a reconstructive transformation when its structure changes and the iron oxide becomes hematite. The oxidation of iron oxides depends on the temperature of the suspension as well as the pH, and the oxygen solubility. Exposure to air is sufficient to oxidize magnetite to maghemite, and at temperatures exceeding 300^{o}C, further to hematite. At low temperatures, near room temperature (25 ^{o}C), the process is slow [16]. As magnetite is oxidized to maghemite, the surface area does not change as it is a topotactic transformation; however, the density and weight decrease due to the loss of iron and the uptake of oxygen. Fe^{II} migrates from the center towards the surface leaving vacancies and incorporating oxygen, while creating a maghemite shell around the particle. During oxidation, the number of iron atoms per unit cell drops from 24 to 21 $^{1}/_{3}$. Oxidation is dependent on the created vacancies for migration. In hydraulic systems, excess water limits the number of vacancies, thereby, inhibiting oxidation. Fe^{II} diffusion has been characterized by a shrinking sphere model [17]. The oxidation rate for smaller particles is faster due to the shorter diffusion path for Fe^{II}. When the particle size is large, the maghemite shell inhibits migration of Fe^{II}, halting or slowing further oxidation. As oxidation proceeds, Fe^{II} concentrations decrease, as proven by dissolving the particles in acid and measuring Fe^{II} [16].

When the Fe^{II} in magnetite is oxidized to Fe^{III}, vacancies are left in its place, without altering the structure, resulting in maghemite. The 32 cubic close packed anions are filled in with 21 $^{1}/_{3}$ Fe^{III} cations and 2 $^{1}/_{3}$ vacancies. In magnetite, Fe^{II} is restricted to

octahedral sites; therefore, the vacancies remaining after oxidation are also confined to the octahedral sites of the crystalline structure [6].

Surface Area

The size of a crystal is dictated by the conditions under which it is formed and particle surface area is directly related to the size of the crystal. When magnetite is synthesized in an aqueous environment, the particles are typically fine-grained rounded, cubic, or octahedral [6]. When OH^- anions are in excess during synthesis (i.e., a pH greater than 12), cubic crystals form, while when iron is in excess, the crystals tend to be spherical [6].

Crystal size can be determined if a crystal can be measured visually by electron microcopy. As particle size decreases, the surface area increases, when expressed by an area to mass ratio ($m^2\ g^{-1}$). This relationship is represented in Figure 2-5. Interaction at the surface of the particle depends on the crystallography and available surface sites of the iron oxide. The surface area of a particle plays a major role in it's dissolution, dehydroxylation, adsorption of sorbents, phase transformations, and thermodynamic stability [6]. High surface area particles are generally formed under low temperatures and high rates of growth, while low surface area particles arise from syntheses at high temperatures and slower growth rates.

The oxidation of magnetite to maghemite usually does not change the surface area because the reaction is topotactic [6]. However, maghemite that forms via other precursors will have a different surface area than its predecessor [6].

Surface Chemistry and Stability

Surficial iron in magnetite coordinates with water in aquatic environments to produce a hydroxylated surface. These hydroxyl groups give magnetite acid/base properties due to the presence of a dissociable hydrogen atom [6]. An increase in pH of a magnetite solution results in a more negative surface, as the hydroxide ions dissociate. Conversely, a decrease in pH results in a more positive charge due to the protonation of the hydroxyl groups. The net charge of a particle is measured by the movement of the particle towards an anode or cathode in a process called electrophoresis. The hydroxide ions adsorbed to the surface of the iron oxide compose what is referred to as the Stern layer. Freely moving counter ions just outside of the Stern layer (SL) are referred to as the diffuse layer (DL), which electrically balances the system. Together the two layers compose what is referred to as the electric double layer depicted in Figure 2-6. The pH at which there is no net movement towards the anode or cathode is called the isoelectric point (iep) or point of zero charge (pzc) and occurs when the net electrostatic charge is neutral. The iep for magnetite has been measured around pH 6.8 and that for maghemite is around pH 6.6 [6]. The magnitudes of these measurements change with temperature, surface impurities, and the adsorption of ions other than H^+ and OH^- [6].

The surface chemistry of iron oxides directly affects its properties [11, 18]. The stability of the iron oxide is described by its ability to remain in suspension. The stability of a magnetite suspension is directly related to the magnitude of the electric double layer. Magnetism can add to a suspension's instability, however, it is considered to be much less dominant than the electric double layer. The thicker the double layer, the more stable the solution will be due to the dominance of repulsive forces. The addition of inert electrolytes into the suspension compresses the double layer, enhancing instability and

potentially promoting floc formation via coagulation. Particles with the same surface charge repulse each other, which inhibits coagulation. Repulsion between magnetite particles is decreased when their surfaces are neutralized by the adsorption of ions and, hence, enhances coagulation. Coagulation can occur when the repulsive energy and/or the electric double layer are decreased enough for the weak van der Waals attractive forces, which are neither electrostatic nor covalent, to dominate the system and create particle flocs. Coagulation is enhanced at pH values near the pzc by eliminating particle to particle repulsion [10]. Once the potential energy barrier is lowered enough for coagulation to occur, the rate will be dependent on the collision rate which in turn is dependent on the concentration of particles and their diffusion coefficients. As coagulation occurs, the available surface area is expected to decrease [6].

Sorption

Adsorption, specific or non-specific, can be measured by the extent to which an adsorbent removes an adsorbate from the media from which it came. Non-specific adsorption occurs between the adsorbate and the surface hydroxyl groups of the iron oxide and the degree to which the adsorbate is removed varies depending on the species involved. Outer sphere adsorption retains solvent between the adsorbate and metal surface. Non-specific adsorption is driven by electrostatic forces. With an increase in pH, non-specific adsorption of anions decreases as the surface charge of the iron oxide becomes more negative. Conversely, a decrease in pH will decrease adsorption of cations as the surface becomes more positive [6].

Specific adsorption is the exchange of a hydrated ligand for the adsorbate ligand. Other terms used for this exchange are chemisorption, inner sphere adsorption, and ligand

exchange. Due to the absence of solvent between the metal and the ligand, the complex has covalent-like properties. Direct adsorption to the surface of the metal allows same charges or neutral charges to specifically adsorb to the surface and for specific adsorption to occur at acidic and basic pH values. Usually pH values approaching or greater than the pK_a of the adsorbate will produce an increase in adsorption by increasing the anion concentration. Non-specific and specific adsorption normally increase as the concentration of adsorbate increases. Specific binding is usually quite durable and can be accomplished by anions such as phosphate, silicate, selenite, arsenite, chloride, fluoride, citrate, and oxalate [6].

Magnetite in Environmental/Engineering Systems

Magnetite is of increasing interest in the environmental engineering field because of its potential for sorption and reduction of contaminants. Nanoscale iron oxides present advantages compared to permeable reactive barriers (PRB) that are currently being employed for remediation of polychlorinated hydrocarbons. PRBs are restricted by the types of sites to which they are applicable and by the shallow depths to which they can reach, while nanoparticles can be directly injected into an area of interest [5]. Not only do nanoscale iron oxides have a practical application aspect, but they are also of interest due to their high surface area to mass ratio.

Arsenic Adsorption

All around the world, arsenic can be found in water systems [4]. The United States has established a drinking water maximum permissible concentration of arsenic to be 10 μg/L. There are numerous current technologies for removing arsenic from water such as membrane filtration and reverse osmosis. Iron oxides are under investigation due

to their high affinity for arsenic [4]. The magnetic properties of magnetite make magnetite/arsenic complex removal of great interest [19]. The oxidation state of arsenic and the pH of the system control adsorption. Arsenic is found in nature as As^{III} or As^{V}. Arsenate, As^{V}, has high affinity for iron oxides at low pH values, while arsenite, As^{III}, adsorbs most efficiently at basic pH values. Arsenite is more common and more detrimental to human health; therefore, arsenite is discussed herein in greater depth. Adsorption of arsenite to magnetite is best described by a Langmuir isotherm that relates the mass of adsorbate adsorbed per mass of adsorbent [4]. Dissolved arsenite is dominated by the neutral species $H_3AsO_3^0$. The neutral charge allows arsenite to bypass the negative surface charge of magnetite at pH values greater than its iep [20]. The adsorption of arsenic involves formation of an inner-sphere bidentate-binuclear complex [4]. As discussed earlier, inner-sphere indicates specific adsorption signifying there is no solvent between the arsenic and the iron oxide. Bidentate-binuclear signifies that the arsenic is bound to two separate iron atoms. Extended X-ray absorption fine structure (EXAFS) spectroscopy and Fourier transform infrared (FTIR) spectroscopy have been used to justify this adsorption mechanism [4]. Studies have been done to investigate adsorption capabilities based on the size (surface area) of the magnetite particles as well as competition between the arsenic and other constituents of water systems such as phosphate, sulfate, silic acid, bicarbonate, and natural organic matter [4]. Results show that as size is decreased that adsorption increases, most likely due to an increase in available surface area sites. In addition, as competitive anion concentrations increased adsorption decreased [4].

Hydrocarbon Reduction

Carbon tetrachloride (CT) plagues many of the groundwater systems of the United States and is listed in the top 7 groundwater contaminates in the Environmental Protection Agency Priority Pollutant List [21]. The fate of carbon tetrachloride is of great concern as some transformation pathways result in production of compounds of greater concern than CT such as chloroform (CF), $HCCl_3$ [15]. One CT reduction pathway, hydrogenolysis, results in as much as 50% formation of chloroform. When magnetite is oxidized, serving as an electron donor; Fe^{II} loses one electron becoming Fe^{III}. When CT acts as the oxidant, or electron acceptor, the molecule can be stripped of a chlorine atom, leaving a free chloride anion and trichloromethyl free radical ($^{\cdot}CCl_3$). Chloroform is produced by the addition of hydrogen to the free radical or to the further reduced product trichloromethyl carbanion ($:CCl_3^-$). Another reduction pathway is carbene hydrolysis which results in carbon monoxide (CO) production. Two electrons donated from magnetite can result in the stripping of two chlorines from CT, leaving dichlorocarbene ($:CCl_2$). Dichlorocarbene quickly hydrolyzes to form CO, and possibly formate ($HCOO^-$). If the dichlorocarbene is reduced instead of being hydrolyzed, methane (CH_4) is formed [15]. A study at Clemson University with magnetite coated zero-valent iron has shown the reduction of CT to be a pseudo first-order reaction that increases with an increase in the chlorinated reactant concentration [5].

The Clemson study also shows the effect of pH on the reduction rates of chlorinated products. Ranges in pH from 6-9.5 showed that the lower pH values had higher reaction rates. This is proposed to be due to possibly higher corrosion rates at lower pH values and also the possibility that higher pH values cause the surface to become more passive [15]. The pH trend is also demonstrated by lower reaction rates in

un-buffered suspensions that produced an increase in pH as time proceeded. As reactions occur, protons can be generated or consumed. To counter the change this will have on the pH of the system, a buffer may be used. Buffers may form a complex with an iron oxide, changing the reactivity by altering reaction sites, accessibility, or the iron oxides' ability to transfer electrons [21]. The presence of organic buffers has shown to increase the amount of chloroform produced in the reduction of carbon tetrachloride [21]. An intermediate, $:CCl_3^-$, acts as a very strong base, able to remove a proton from water or from most organic buffers in the neutral pH range forming CF [21]. TRIS (tris(hydroxymethyl) aminomethane) has shown to enhance reactivity of magnetite and CT by possibly increasing accessibility of CT to the reactive surface sites or by increasing magnetite's ability to transfer electrons [21]. Reaction rates can also increase due to the inhibitory aggregation effects that certain buffers have on magnetite particles [21].

A study has shown that reaction rates are up to four times greater for nano-sized iron than for micro-sized, which is attributed to an increase in surface area [5]. However, nano-sized particles tend to agglomerate, resulting in a loss of surface area and reactivity [22]. Particles can tend not be readily dispersed and aggregate due to high surface energies and particle-particle attraction of van der Waals forces [7]. An Auburn study has shown that zero-valent iron, Fe^0, nanoparticles produced with a starch that acts as a stabilizer was able to reduce 80% of polychlorinated biphenyls, PCBs, while particles without the stabilizer agglomerated and settled, reducing the PCBs by only 24% [22]. Slow and incomplete dechlorination can produce hazardous byproducts [22]. Stabilization is also important to obtain particle flow through soils for remediation by

avoiding aggregation [23]. From an engineering standpoint, manipulation of iron oxides, including magnetite, would be extremely beneficial to avoid agglomeration to aid its transport through a media to a desired area where a disperse reaction would maximize remediation [7].

References

1. Wang, L.Y., et al., *One-pot synthesis and bioapplication of amine-functionalized magnetite nanoparticles and hollow nanospheres.* Chemistry-a European Journal, 2006. **12**(24): p. 6341-6347.
2. Vikesland, P.J., et al., *Particle size and aggregation effects on magnetite reactivity toward carbon tetrachloride.* Environmental Science & Technology, 2007. **41**(15): p. 5277-5283.
3. Heathcock, A.M., *Characterization of Magnetite Nanoparticle Reactivity in the Presence of Carbon Tetrachloride*, in *Civil and Environmental Engineering*. 2006, Virginia Polytechnic and State University: Blacksburg. p. 50.
4. Yean, S., et al., *Effect of magnetite particle size on adsorption and desorption of arsenite and arsenate.* Journal of Materials Research, 2005. **20**(12): p. 3255-3264.
5. Song, H. and E.R. Carraway, *Reduction of chlorinated methanes by nano-sized zero-valent iron. Kinetics, pathways, and effect of reaction conditions.* Environmental Engineering Science, 2006. **23**(2): p. 272-284.
6. R.M. Cornell, U.S., *The Iron Oxides Structure, Properties, Reactions, Occurrences and Uses*. Second ed. 2003: Wiley-VCH Verlag GmbH & Co. KGaA, Weinheim. 664.
7. Saleh, N., et al., *Adsorbed triblock copolymers deliver reactive iron nanoparticles to the oil/water interface.* Nano Letters, 2005. **5**(12): p. 2489-2494.
8. Shebanova, O.N. and P. Lazor, *Raman study of magnetite (Fe3O4): laser-induced thermal effects and oxidation.* Journal of Raman Spectroscopy, 2003. **34**(11): p. 845-852.
9. Yu, W.W., et al., *Aqueous dispersion of monodisperse magnetic iron oxide nanocrystals through phase transfer.* Nanotechnology, 2006. **17**(17): p. 4483-4487.
10. Vayssieres, L., et al., *Size tailoring of magnetite particles formed by aqueous precipitation: An example of thermodynamic stability of nanometric oxide particles.* Journal of Colloid and Interface Science, 1998. **205**(2): p. 205-212.
11. Jolivet, J.P., C. Chaneac, and E. Tronc, *Iron oxide chemistry. From molecular clusters to extended solid networks.* Chemical Communications, 2004(5): p. 481-487.
12. Kohn, T., et al., *Longevity of granular iron in groundwater treatment processes: Corrosion product development.* Environmental Science & Technology, 2005. **39**(8): p. 2867-2879.
13. Zhang, Z., et al., *Effect of pipe corrosion scales on chlorine dioxide consumption in drinking water distribution systems.* Water Research, 2008. **42**(1-2): p. 129-136.
14. McCormick, M.L., E.J. Bouwer, and P. Adriaens, *Carbon tetrachloride transformation in a model iron-reducing culture: Relative kinetics of biotic and abiotic reactions.* Environmental Science & Technology, 2002. **36**(3): p. 403-410.
15. Hanoch, R., H. Shao, and E.C. Butler, *Transformation of carbon tetrachloride by bisulfide treated goethite, hematite, magnetite, and kaolinite.* Chemosphere, 2006. **63**(2): p. 323-334.

16. Tang, J., et al., *Magnetite Fe3O4 nanocrystals: Spectroscopic observation of aqueous oxidation kinetics.* Journal of Physical Chemistry B, 2003. **107**(30): p. 7501-7506.
17. Sidhu, P.S., R.J. Gilkes, and A.M. Posner, *Mechanism of Low-Temperature Oxidation of Synthetic Magnetites.* Journal of Inorganic & Nuclear Chemistry, 1977. **39**(11): p. 1953-1958.
18. Sun, Z.X., et al., *Surface characteristics of magnetite in aqueous suspension.* Journal of Colloid and Interface Science, 1998. **197**(1): p. 151-159.
19. Yavuz, C.T., et al., *Low-field magnetic separation of monodisperse Fe3O4 nanocrystals.* Science, 2006. **314**(5801): p. 964-967.
20. Wood, S.A., C.D. Tait, and D.R. Janecky, *A Raman spectroscopic study of arsenite and thioarsenite species in aqueous solution at 25 degrees C.* Geochemical Transactions, 2002. **3**: p. 31-39.
21. Danielsen, K.M., J.L. Gland, and K.F. Hayes, *Influence of amine buffers on carbon tetrachloride reductive dechlorination by the iron oxide magnetite.* Environmental Science & Technology, 2005. **39**(3): p. 756-763.
22. He, F. and D.Y. Zhao, *Preparation and characterization of a new class of starch-stabilized bimetallic nanoparticles for degradation of chlorinated hydrocarbons in water.* Environmental Science & Technology, 2005. **39**(9): p. 3314-3320.
23. Schrick, B., et al., *Delivery vehicles for zerovalent metal nanoparticles in soil and groundwater.* Chemistry of Materials, 2004. **16**(11): p. 2187-2193.

Tables and Figures

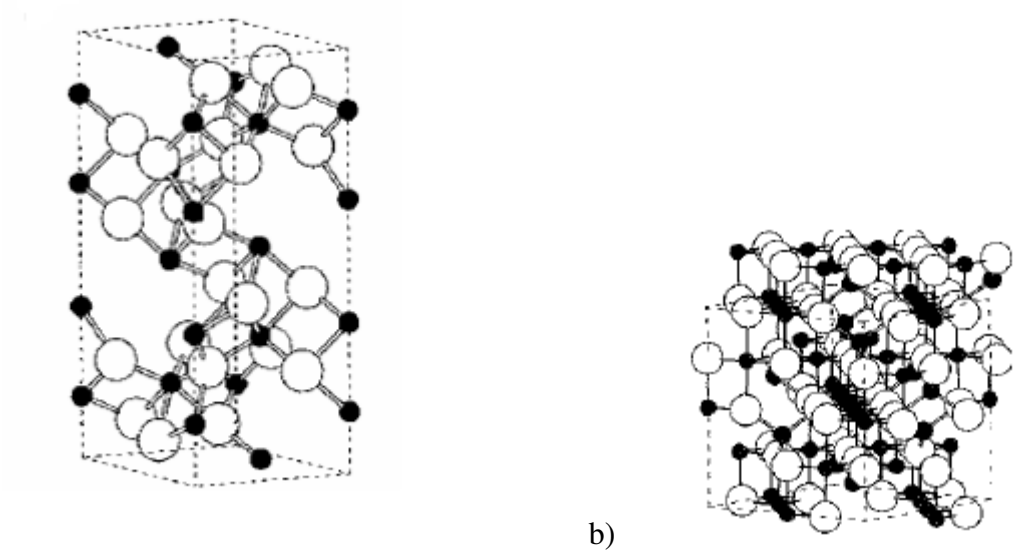

a) b)

Figure 2-1. Crystalline structures for a) hematite and b) magnetite and maghemite. With permission, R.M.Cornell. The Iron Oxides Structure, Properties, Reactions, Occurrences and Uses. 2003. Wiley-VCH Verlay GmBH & CoCo.

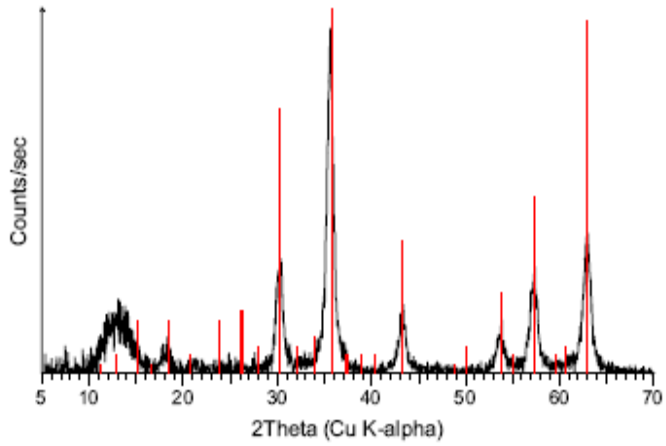

(a)

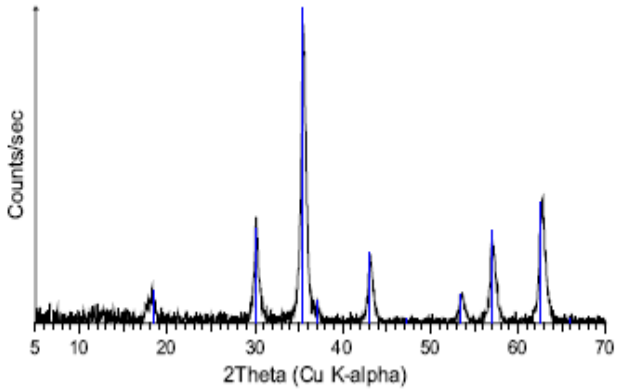

(b)

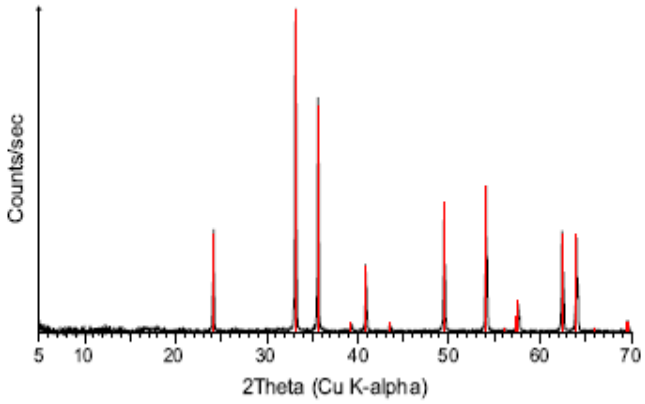

(c)

Figure 2-2. X-ray Diffraction for (a) magnetite, (b) maghemite, (c) hematite. This article was published in Dyes and Pigments, Vol 74, Legodi, M.A., and D. de Waal. The preparation of magnetite, goethite, hematite and maghemite of pigment quality from mill scale iron waste. Page 161-168, Copyright Elsevier 2007.

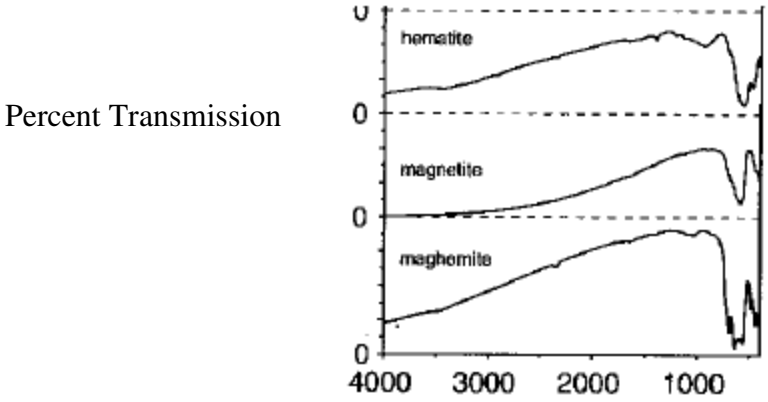

Figure 2-3. Infrared Spectroscopy. With permission, R.M.Cornell. The Iron Oxides Structure, Properties, Reactions, Occurrences and Uses. 2003. Wiley-VCH Verlay GmBH & CoCo.

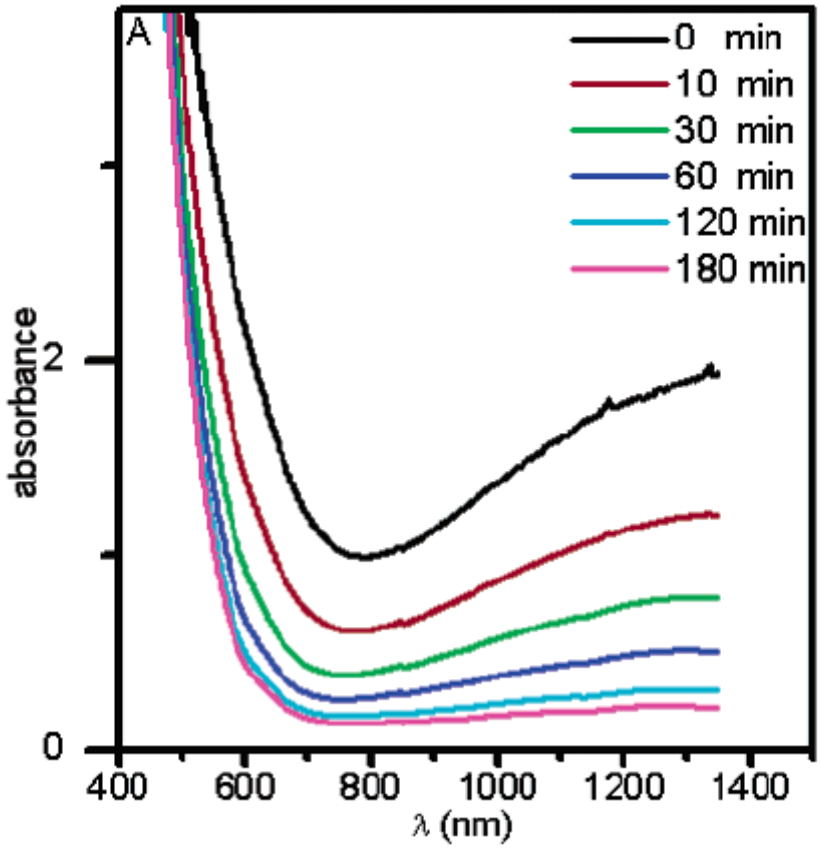

Figure 2-4. UV-Vis-NIR spectroscopy for the oxidation of magnetite at 80°C. With permission. Tang, J., et al., *Magnetite Fe3O4 nanocrystals: Spectroscopic observation of aqueous oxidation kinetics.* Journal of Physical Chemistry B, 2003. 107(30): p. 7501-7506.

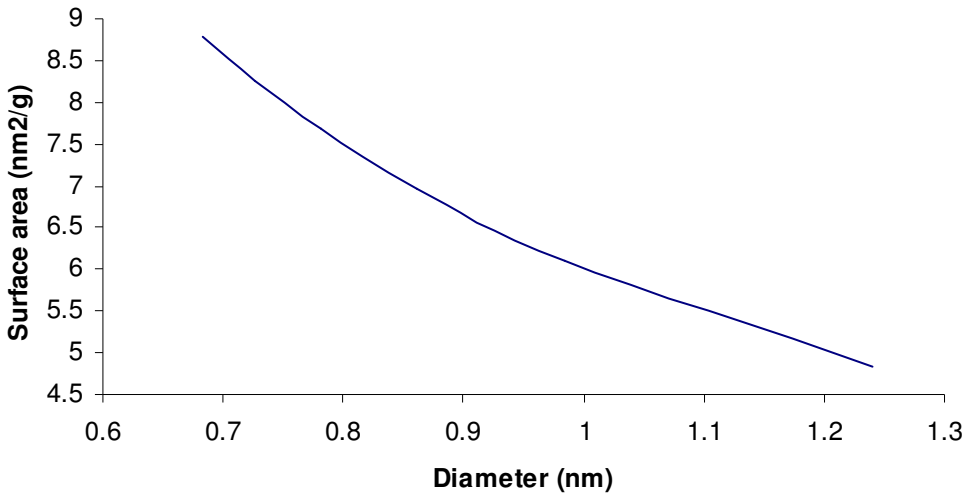

Figure 2-5. Surface area vs. diameter representation at constant particle volume and mass.

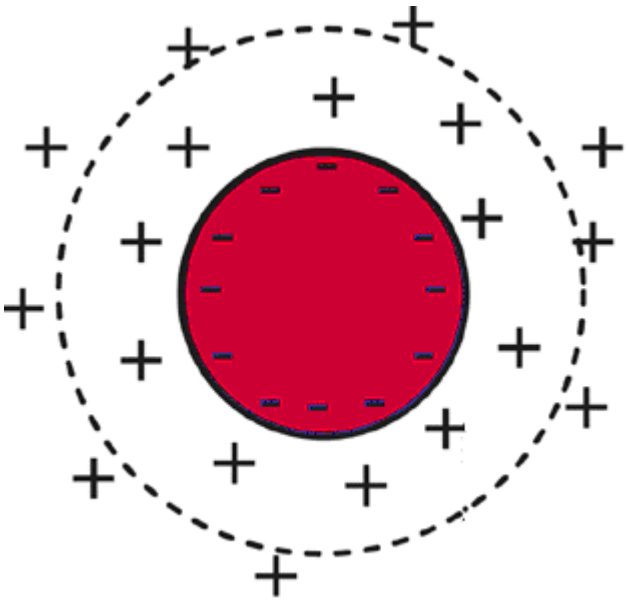

Figure 2-6. Electric Double Layer

III. Monitoring Magnetite Oxidation by Use of UV-Vis-NIR Spectroscopy

Introduction

Environmental engineering has been investigating the properties of magnetite and other iron oxides for years [1-3]. The abundance of iron oxides in natural systems and their specific structural and surface chemistry have led to the investigation of iron oxide anthropogenic uses. Over the course of human advancement, iron oxide uses have developed from simple cave drawings using iron oxide pigmentation to advanced water treatment uses [4]. The properties of nanoscale magnetite have become an area of interest in research for the purpose of the remediation of groundwater contaminates such as arsenic and chlorinated hydrocarbons [1, 5].

Magnetite does not remain stable within the natural environment, as exposure to oxidants, such as oxygen, and temperature increases can transform magnetite into other iron oxides. As magnetite is oxidized it undergoes a topotactic transformation to maghemite. The rate at which this transformation occurs greatly depends on the temperature at which magnetite is oxidized [6]. Numerous studies have identified magnetite and maghemite as well as many other iron oxides by the use of different types of spectroscopy and diffraction [4, 7]. Diffraction methods, such as X-ray diffraction, are limited by the fact that the crystalline structure of maghemite and magnetite are the same [4]. The use of Raman spectroscopy has proven effective for identifying the different iron oxides; however, little has been done to monitor the transformation of one iron oxide to another by Raman spectroscopy analysis [7]. This study aids in the characterization of the transformation kinetics of magnetite to maghemite by employing UV-Vis-NIR spectroscopy.

UV-Vis-NIR spectrometer produces the energy required, by use of a tungsten lamp, to cause transitions with a sample. These transitions are valence electron excitations that are specific to the compound being analyzed. Magnetite is comprised of divalent iron (Fe^{II}) and trivalent iron (Fe^{III}). Studies by Tang et al. have monitored the change in absorption due to the transitions in NIR-region by to the decreasing interactions between Fe^{II} and Fe^{III} [6]. Due to their unequal quantities of valence electrons, an electron is excited, hopping between Fe^{II} and Fe^{III} and it is this transition that is measured by the UV-Vis-NIR in the NIR-region. The decrease in absorption due to magnetite has been monitored; however, it is in this study that monitors the increasing absorption due to maghemite within the UV-region as well. The transition which causes the increased absorption in the UV-region is between magnetically coupled Fe^{III}, which correlates to an increase in maghemite concentration. For this study, the rate at which magnetite is transformed to maghemite is dependent only on temperature as all other parameters that effect oxidation are constant between the trials, such as pH and oxidant concentrations (in this study oxygen). The temperature at which magnetite and maghemite is measured also contributes to the intensities of absorption and other UV-Vis-NIR spectra characteristics. By investigating the kinetics of oxidation of magnetite, future studies of magnetite reactivity, especially in oxidation/reduction reactions can be better interpreted.

Materials and Methods

De-aerated water was used for the synthesis of magnetite and for all experiments. Deionized water (>18.1 MΩ) from a Barnstead Nanopure filtration system was boiled for approximately 50 minutes; halfway through this period the water was sparged with argon

gas while continuing to boil. The de-aerated water was capped, cooled, and stored within an anaerobic glovebox (Coy Laboratory Products Inc.) until it was used. All chemicals employed were reagent grade from Fisher Scientific of Sigma-Aldrich.

Particle Synthesis. Magnetite was synthesized in an anaerobic glovebox with an atmospheric composition of 95%/5% N_2/H_2. Particles were prepared by a method established by Vayssieres et al. involving the co-precipitation of divalent iron (Fe^{II}) and trivalent iron (Fe^{III}) [8]. In brief, a base solution of 1 M sodium hydroxide and 1 M sodium chloride was continually stirred, while an iron solution was added dropwise. The iron solution was comprised of 0.1 M ferrous chloride mixed with an equal volume of 0.2 M ferric chloride. Particles coated with the stabilizer tetramethylammonium hydroxide (TMAOH) were synthesized in a similar manner; however, with 1 M TMAOH as the basic medium instead of sodium hydroxide [6]. All chemicals were weighed outside of the anaerobic chamber, but the final solutions were prepared within the chamber using de-aerated water. The volumetric ratio of iron to base was held at 3:2 with a pH value above 12. Throughout the addition of the iron to the base, an overhead mixer, stirring rod and PTFE stirring blade rapidly mixed the suspension. Upon completion of the magnetite synthesis, the particles were separated from the background solution using a magnet. The supernatant was decanted and repeatedly replaced with de-aerated water to remove excess salts. The washed magnetite particles were stored in the anaerobic chamber in a polypropylene container in de-aerated water at a pH of approximately 10.

The mass concentrations of the magnetite solutions were determined by drying a specific volume aliquot of the well mixed suspension in an oven at 75 ^{o}C. The mass of the dry iron oxide along with the known sample volume enabled calculation of a mass

concentration (g/L) representative of the entire production's magnetite suspension. When the sample dries, it is assumed that the magnetite is completely oxidized to maghemite. This assumption was used to convert the mass concentration to a molar concentration as described by Heathcock [5].

When the magnetite suspensions were stored over extended periods of time, the particles agglomerated [8]. To avoid conducting experiments with aggregated particles, prior to the initiation of any experiment, the stock suspension of magnetite was well mixed and the experimental aliquots of magnetite were briefly sonicated ($t < 1$ minute) to breakup aggregates and re-suspend the particles.

Oxidation Experiments. Prior to initiating an oxidation experiment, the magnetite particles were maintained under strictly anaerobic conditions. An oxidation experiment was started by transferring 250 mL of magnetite suspension to a three neck flask in the inert atmosphere of the glovebox. This flask was then sealed with rubber stoppers and removed from the glovebox. The anaerobic suspensions where shaken by hand and sonicated for approximately one minute to break up aggregates. The oxidation experimental setup was comprised of a three-neck flask, a glass diffuser rod, and a condenser. House air was bubbled through the suspension using the air diffuser in the side stem of the flask, which rested on the bottom-center of the flask. The middle neck of the flask was occupied by the condenser, while the other two necks were sealed off with rubber stoppers. One of the rubber stoppers was penetrated by a stainless steel sampling tube and a thermocouple. The thermocouple was attached to a Cole-Palmer Temperature Controller that regulated the temperature of the system by controlling the Barnstead Electrothermal heating mantle on which the three neck flask rested. To insulate the

system, the flask was wrapped in aluminum foil, helping maintain the desired temperature of the system. The setup is shown in Figure 3-1. Analysis by the UV-Vis-NIR spectrometer required a low concentration; therefore, the concentration used was approximately 2 mM.

Sampling for the UV-Vis-NIR spectroscopy analysis was by withdrawing approximately 3 mL for each analysis which was immediately placed into a 1 cm quartz cuvette and measured.

UV-VIS-NIR Spectrometer. Using a temperature controller, the temperature of the Cary 5000 UV-VIS-NIR spectrometer was set to the same temperature as the oxidation setup. Absorbance was measured over a spectral range of 400-1350 nm. Magnetite absorption begins in the near IR range of 800 nm to 2500 nm. At approximately 1400 nm the measurements are dominated by the background solution; therefore, the range was limited to 1350 nm. The entire range was measured in approximately 3 minutes by the spectrometer which was set to repeat the measurements for 20 minutes.

Results and Discussion

Particle synthesis. Particles synthesized by the production method outlined in the Materials and Methods were characterized extensively by Heathcock. The method confidently produces nanoscale magnetite [5]. For this effort, in contrast to the work of Heathcock, magnetite was synthesized using TMAOH as the base medium instead of NaOH. Particles synthesized using TMAOH were characterized by Tang et al. and show the same characteristics as particles formed in NaOH, except they are more stable in

suspension [6]. As expected for magnetite, the product was dark black and highly responsive to a magnet.

Oxidation. The oxidation setup (Figure 3-1) was successful for oxidizing magnetite. During the oxidation period, the dark black magnetite gradually changed to a red-brown color indicative of maghemite. Figure 3-2 shows the change in color due to oxidation. To quantitatively monitor the oxidation process, samples were periodically drawn and subjected to UV-Vis-NIR spectroscopy.

UV-Vis-NIR spectroscopy. UV-Vis-NIR uses ultraviolet, visible, and infrared light to excite valence electrons in a sample from the ground state to an excited state. The spectrometer then quantifies the amount of light that is allowed to pass through the sample. This transmittance measurement in then readily converted into an absorbance. Different wavelengths have energies that produce specific transitions within a molecule.

In an iron oxide there are different types of possible transitions. The valence electrons of iron are in the *d* orbitals. The 5 *d* orbitals, depicted in Figure 3-3, can be separated into different groups with different energy levels when in the presence of the electron cloud of oxygen as in iron oxides. The transitions that occur due to the tungsten quartz halogen lamp occur as an electron is excited from one *d* orbital into another *d* orbital. One transition is a Fe^{III} ligand field transition [4]. When one Fe^{III} atom is magnetically coupled to a neighboring Fe^{III} atom, two Fe^{III} ligand field transitions are excited simultaneously, raising absorption intensities [10]. Magnetic coupling of the electronic spins in neighboring Fe^{III} allow for these intense transitions to occur. Magnetic coupling is further explained later when ferromagnetism is discussed. Typically, Fe^{III} ligand field transitions result in absorbencies over the wavelength range of 290-380 nm.

Another type of electronic transition that occurs in iron oxides and that can be probed by UV-Vis-NIR spectroscopy involves charge transfer either between Fe^{III} and oxygen or Fe^{II} and Fe^{III} [4]. In the case of magnetite, which contains both Fe^{III} and Fe^{II}, the Fe^{II} has one more electron than Fe^{III}; therefore, the Fe^{II} can act as an electron donor and the Fe^{III} can act as an electron acceptor. The electron hops between the iron atoms causing a Fe^{II}-Fe^{III} electron hopping transition. Typically, Fe^{II}-Fe^{III} intervalence charge transfer transitions result in absorbencies within the visible wavelength range or 600-900 nm; however, the major absorption band occurs at approximately 1500 nm [4, 6]. Charge transfer transitions can also occur between the oxygen and iron within a molecule. The electron is excited and transferred through a molecular orbital formed by the two atoms. Intersublattice charge transfer transitions are also possible as an electron is excited from an octahedral coordination site to a tetrahedral coordination site or from a tetrahedral to an octahedral site. Charge transfer transitions are responsible for the majority of the absorption in the visible-region of the spectra [4]. Once the electrons are in their excited states they return to their ground states by two possible relaxation processes [11]. The most typical relaxation pathway involves the loss of heat from the excited state [11]. Another pathway is a photochemical reaction that actually produces a new species. In UV-Vis-NIR these excitations/transitions are created by the absorption of photons from the light source.

Magnetite absorbs throughout the UV-Vis-NIR region and is one of only two iron oxides that absorbs in the NIR-region, the other being wustite which was absent from this study and thus irrelevant for further discussion. Maghemite strongly absorbs in the UV-region, but has almost no absorption above 700 nm [12]. These differences in the

absorption characteristics of magnetite and maghemite make it possible to readily observe magnetite oxidation by UV-Vis-NIR spectroscopy. In this study the spectrometer was set to measure absorbance over the spectral range of 400-1350 nm. The samples were repeatedly scanned for 20 minutes with individual scans each lasting approximately 2 minutes. For the majority of the UV-Vis-NIR experiments, the measurement chamber of the spectrometer was set to the same temperature as was employed for a given oxidation experiment. The concentration needed for UV-Vis-NIR spectroscopy is quite low so an initial magnetite concentration of 2 mM was used at a pH of approximately 8. Low concentrations are needed for UV-Vis-NIR analysis due to the direct effect that concentration has on absorption. Too high of a concentration greatly diminishes light transmission through the sample which will falsely alter the measured absorptions.

Absorption Spectra Characteristics. Figure 3-4 shows the first and second scans acquired at the initiation (t=0) of oxidation experiments at 60, 70, and 80 °C. In the near-IR (NIR) region the absorption of magnetite dominates the absorption spectra. Magnetite has a prominent absorption around 0.8 eV, or 1500 nm, in the NIR region [4]. However, in aqueous suspensions an absorption band for water begins to affect the spectrum at ~ 1400 nm. At wavelengths up to 1350 nm, the beginning of the magnetite band is visible. As discussed in Chapter 2, magnetite's octahedral sites are occupied by Fe^{II} and Fe^{III}. The absorbance band of magnetite at 0.8 eV results from electron hopping that occurs between Fe^{II} and Fe^{III} in neighboring octahedral sites [4]. This band is referred to as an intervalence charge transfer (IVCT) band [13].

Octahedral Fe^{III} transitions that are magnetically coupled to neighboring Fe^{III} atoms have absorptions that are very intense at wavelengths below 600 nm. The majority of the absorption in the range of 600 nm to 900 nm charge transfer transitions between Fe^{III} and oxygen as well as the charge transfer between Fe^{II} and Fe^{III}. Both maghemite and magnetite contribute to the absorption in the visible-region as the Fe^{III}-O interactions are present within both iron oxides. The transition absorptions at wavelengths between 600 and 900 nm are less intense than the absorption edge created by the Fe^{III}-Fe^{III} transition absorption in the UV region. The absorption edge begins to increase in absorption as the weaker bands arise, causing absorption to slightly increase as the NIR is approached where the peak absorption of the Fe^{II}-Fe^{III} charge transfer transition occurs.

Maghemite has a threshold optical absorption at approximately 2 eV, or 620 nm, which is in the visible region of the spectrum [6]. The maxima for this absorption band is found in the ultraviolet region at a wavelength below the range used in the oxidation experiments. For the particle concentrations employed in these studies, as the spectrometer approached 400 nm, sample absorption became too large to be accurately quantified. The intense absorption band in the UV range results from the transitions of magnetically coupled octahedral Fe^{III} [10]. For the initial measurements at each temperature, there is no maghemite present within the sample and thus absorption within this region is due to Fe^{III} transitions within magnetite. All iron oxides absorb in this region; however, monitoring changes in the absorption of this UV-region band is an effective way to observe the change in the maghemite concentration within the sample.

Differences Between Repetitive Scans. Upon casual evaluation of Figure 3-4 it is apparent that within the magnetite region of the spectrum there are significant differences

between the first and second scans at each of the tested temperatures. The first scan appears to have two "humps", the smaller "hump" having an absorption maxima at approximately 1058 nm and the larger "hump" with an absorption maxima at 1260 nm. These peaks are not present in the second scan of the same sample. The differences between these two scans were observed at all three temperatures and at each stage of an oxidation experiment and are thus not experimental artifacts. The differences are due to the Fe^{II}-Fe^{III} charge transfer transition characteristics at these wavelengths. When light from the tungsten quartz halogen lamp of the spectrometer interacts with the sample, these Fe^{II}-Fe^{III} transitions are excited, albeit only temporarily. As a result of thermal charge transfer, the absorbance in the first scan is quickly lost as the transition settles back to its ground state [13]. This settling from an excited energy state back to the ground state accounts for differences in absorption between repetitive scans in the magnetite region. This trend continue for all of the scans performed during a given measurement period. Further discussion of magnetite concentration/absorption will be discussed with respect to the changes that occur in the peak at 1260 nm.

In Figure 3-5, the change in absorption of the sequential scans from the t=0 samples are presented. In this figure it can be seen that the difference between the later scans decreases, leading to the belief that there is a minimum absorption that would eventually have been reached if the scans were allowed to continue within the same sample. This final absorption could possibly be the ground state to which the excited transition returns through the thermal charge transfer.

In the Fe^{III}-Fe^{III} transition region (<600 nm), the absorptions are very similar from scan to scan within the same sample. This suggests that the tungsten quartz halogen lamp

used to excite the samples has a greater effect on Fe^{II}-Fe^{III} electron hopping than on Fe^{III}-Fe^{III} transitions. In the first scan, the maximal absorption within the magnetite region occurs at approximately 1260 nm. This wavelength was selected to evaluate magnetite absorption/concentration during the oxidation studies.

Temperature Effects on Spectra. Molar absorptivity is a compound characteristic that indicates to what degree a specific wavelength is absorbed by a sample. Molar absorptivity is dependent on the temperature at which the sample is measured [11]. To demonstrate the effect of temperature on the molar absorptivity of magnetite, absorptions for both scan 1 and scan 2 at 1260 nm, from Figure 3-4, were compared for 60, 70, and 80 ^{o}C. At 80 ^{o}C the initial absorption of magnetite (scan 1, 1260 nm) was 1.458. This value decreased by 2.7% to 1.418 at 70 ^{o}C, and by 4.9% to 1.386 at 60 ^{o}C. When the second scan was analyzed in a similar manner, the same trends were noticed; however, to a lesser degree. From 80 ^{o}C to 70 ^{o}C, there was only a 0.7% decrease in absorption at 1260 nm. From 80 ^{o}C to 60 ^{o}C, there was a 1.9% decrease. When the absorptions for scans 1 and 2 are plotted versus the inverse of their respective temperatures, a linear relationship was found as in Figure 3-6. These trends show that higher temperatures enhance the initial excitation (scan 1) of the Fe^{II}-Fe^{III} transitions, but that temperature has a lesser effect on settling back to the ground state as scan 2 had absorptions at 1260 nm that were similar for all three temperatures.

The effects of temperature on absorption for scans 1 and 2 were also analyzed at 450 nm in the Fe^{III}-Fe^{III} transition region. The absorption at 80 ^{o}C was 3.641 in the first scan. As the temperature of measurement dropped to 70 ^{o}C, the absorption dropped 2.3% to 3.556. The absorption at 60 ^{o}C actually increased 6.3% to 3.870 relative to 80 ^{o}C. In

the second scan the absorption dropped 2.4% from 80°C to 70 °C. From 80 °C to 60 °C, the absorption increased 5.4%. When the absorptions are graphed versus the inverse of the temperature no definite relationship can be seen in Figure 3-6; however, in the final oxidation samples a linear relationship is seen as the Fe^{III}-Fe^{III} transition should be at its maximum due to the increase of Fe^{III}. Figure 3-7 depicts the effect of temperature on the transitions when they are at their maximum concentrations. Both wavelengths show a dependence on temperature. The degree to which 450 nm is affected is much greater than that of 1260 nm; however, the temperature effect at 1260 shows a more linear relationship than that at 450 nm. The significance of the data is presented in Appendix A.

Oxidation Experiment Analysis. As oxidation proceeds, the concentration of magnetite decreases, while the concentration of maghemite increases. This trend is represented in the UV-Vis-NIR spectra by a decrease in absorption in the NIR-region and an increase in absorption in the UV-region. As stated previously, only the edges of the magnetite and maghemite absorption bands are visible within the 400-1350 nm spectral window. Monitoring a decrease in the absorption of the magnetite band in the NIR-region enables the evaluation of the changing concentration of magnetite, while monitoring an increase in absorption in the UV-region enables the evaluation of the changing concentration of maghemite.

As magnetite oxidizes, the Fe^{II}, which is only present in octahedral sites, migrates and is oxidized to Fe^{III}, leaving only vacancies and Fe^{III} in those octahedral sites. The decreasing concentration of Fe^{II} restricts electron hopping, thus resulting in lower absorption in the NIR-region. Oxidation increases Fe^{III} concentrations and absorption due to the transitions of octahedral Fe^{III}. The maghemite absorption increase in the UV-

region and the decrease of magnetite absorption in the NIR-region as time progresses is illustrated in Figures 3-8, 3-9, and 3-10.

Scans. As shown in Figures 3-8, 3-9, and 3-10, each sample was typically scanned nine sequential times over a 20 minute period. Figure 3-11 shows, just as in Figure 3-5, that as the change is absorption from one scan to the next is analyzed with a single sample, the difference begins to decrease and level off. Had the scans been allowed to continue for longer than the 20 minute measurement period for each sample, it is likely that the sample would have ultimately reached its ground state energy level which would be indicated by overlapping scans. This trend in the absorption change between scans holds for all of the temperatures and for each oxidation time studied. The figure also shows that in highly oxidized samples that there is less change in absorption between the first scan and the last scan than for a less oxidized sample. In oxidized samples, the Fe^{II} concentration is lower, resulting in less Fe^{II}-Fe^{III} electron hopping. As electron hopping decreases, so should the energy gradient between the excited state and the ground state, which is indicated in the scans of the more oxidized samples.

Figure 3-12 shows that the reaction kinetics obtained by comparing the same scan number for samples obtained at different oxidation times (e.g., scan 1 vs. scan 1, scan 2 vs. scan 2, etc…) are very similar. Even though there are differences from one scan to the next for a given sample, comparisons of the same scan from one sample to the next gives kinetic parameters comparable to other scans; therefore, the scan chosen for kinetics analysis will have minimal bearing on the results of that analysis. In the discussion that follows, the second scan was chosen from each 20 minute scan cycle.

Quantification of Temperature Effects. In Figures 3-8, 3-9, and 3-10, it is noticeable that there are wavelengths where the absorptions for the samples cross irrespective of oxidation time (Figures 3-8b, 3-9b, and 3-10b). This point of intersection is referred to as an isosbestic point. It is considered that wavelengths shorter than the isosbestic wavelength generally correspond to the Fe^{III}-Fe^{III} charge transfer band and wavelengths longer than the isosbestic point are representative of Fe^{II}-Fe^{III} transitions. The isosbestic point is on the downward slope of the Fe^{III}-Fe^{III} charge transfer band. The isosbestic point is the wavelength at which the Fe^{III}-Fe^{III} transitions and the Fe^{II}-Fe^{III} transitions have equal absorptions. As discussed previously, absorption in the Fe^{III}-Fe^{III} transition region of the spectrum is temperature dependent. Upon evaluation of Figures 3-8, 3-9, and 3-10 it is apparent that as the temperature increases the isosbestic point shifts towards shorter wavelengths and is accompanied by an absorption decrease in the UV-region. At 80 ^{o}C the isosbestic point is at approximately 490 nm. The isosbestic point shifts to 545 nm when the temperature is decreased to 70 ^{o}C, a 11.2% change. At 60 ^{o}C, the isosbestic point shifts to 560 nm, a 14.3% change. As temperature decreases, the isosbestic point shifts towards longer wavelengths with lower energy due to an increase in absorption of Fe^{III}-Fe^{III}.

As oxidation proceeds, the magnetite concentration decreases as shown by a decreasing absorption in the NIR-region. At 80 ^{o}C the absorption at 1260 nm in scan 2 falls from 1.335 to 0.884, a 33.8% change. There is a 36.5% change from 1.326 to 0.842 at 70 ^{o}C. The oxidation at 60 ^{o}C drops the absorption from 1.309 to 0.888, a change of 32.2%. The relatively close degrees of final absorption loss indicated that the extent of

oxidation should be quite similar despite the different temperatures and rates at which they oxidized the magnetite.

At the initiation of the oxidation experiments (t=0), there is no maghemite present in the sample. As the sample oxidizes (t > 0 min), the concentration of maghemite increases and the UV absorption band corresponding to the Fe^{III}-Fe^{III} transition increases in magnitude. By evaluating the increase in the absorption of this band as a function of oxidation time it is possible to determine the effect of temperature on the oxidation kinetics as well as the molar absorptivity of maghemite. To observe the change in the molar absorptivity of maghemite, the wavelength 450 nm was chosen for the second scan due to its position in the near UV-region and the fact that it is below the isosbestic points for all temperatures. At the initiation of oxidation at 80 ^{o}C the absorption in the Fe^{III}-Fe^{III} transition region for scan 2 was 3.646 which increased to 3.792 by the end of oxidation three hours later, an increase of 4%. At 70 ^{o}C there was an increase in absorption from 3.556 to 4.023 (13.1% increase) by the end of oxidation. The absorption at 60 ^{o}C increased from 3.843 to 4.753 (23.7% increase) in 10 hours of oxidation.

Comparing the change in absorbance at 450 nm at the termination of the oxidation experiments it can be seen that there is a greater increase in absorption at the low temperatures than at higher temperatures. At the termination of the oxidation, the maghemite concentrations should be equal at all temperatures even though they were run for different periods of time. The final absorption values in the Fe^{II}-Fe^{III} region of the spectrum were similar (the highest difference in absorption between two temperatures being 5.5%) thus signifying that the degree of oxidation between trials was the same and thus the maghemite concentrations should also be equal. Equal concentrations would

result in equal absorptions; however, the large discrepancies in absorption between the samples obtained at different temperatures signify that temperature greatly alters the molar absorptivity of maghemite. It was shown earlier that in the UV-region there was little effect of temperature in the initial samples when there was no maghemite present in the sample (t=0). When the end of oxidation is analyzed (t=x), it can be seen that from 80 ^{o}C to 70 ^{o}C, there is an increase in absorption of 6.9%. From 80 ^{o}C to 60 ^{o}C, shows an increase of 25.3%. These trends clearly show that as the measuring temperature decreases, the molar absorptivity increases for maghemite.

Maghemite and magnetite are ferrimagnetic. A ferrimagnetic compound has no less than two sublattices each of which have an alignment of spins that are antiparallel with unequal moments. Magnetic coupling of Fe^{III} in maghemite and magnetite produces a higher intensity absorption than iron oxides that do not have magnetic coupling [10]. Figure 3-13 shows the strict order of the electron spins in ferrimagnetic and ferromagnetic compounds. As temperature rises this arrangement disassembles in ferromagnetic compounds due to thermal fluctuations of the magnetic moments [4]. It is proposed that temperature has the same effect on ferrimagnetic compounds as it does on ferromagnetic compounds due to magnetic dependence on spin arrangement [4]. At room temperature (298 K) maghemite is ferromagnetic, but above its Curie temperature (between 820 K and 986 K) it loses its ferrimagnetism [4]. Disarrangement as temperature rises would decrease the ferrimagnetism of the iron oxide. The higher the temperature the more of a negative effect imposed on the alignment of spins, possibly inhibiting ferrimagnetism and dampening the absorbance and molar absorptivity of maghemite.

Upon evaluating the absorption data for magnetite and maghemite it can be hypothesized that temperature has a greater effect on the magnetically coupled Fe^{III}-Fe^{III} transitions than on Fe^{II}-Fe^{III} electron hopping. The effect was also the opposite in magnetite and maghemite. In maghemite, lower temperatures produce an increase in molar absorptivity, while in magnetite; the lower temperatures result in lower molar absorptivities. The shift of the isosbestic point towards lower energy/longer wavelengths at lower temperatures supports that the degree to which maghemite is affected by temperature is greater than the effect on magnetite. Table 3-1 presents a summary of the absorptions at 1260 nm, 450 nm, and the isosbestic points for all temperatures.

Application of Beer's Law. By monitoring the change in sample absorbance at 450 and 1260 nm, we were able to monitor relative changes in the concentrations of magnetite and maghemite. Decreases in absorption at 1260 nm signify the oxidation of magnetite, while an increase in absorption at 450 nm corresponds to an increase in maghemite concentration. Using data collected from the second scan at each timepoint, changes were monitored relative to their initial values at the start of an oxidation experiment. When the changes in absorption at 1260 nm are plotted versus the change in absorption at 450 nm, a linear relationship is seen in Figure 3-14. The slopes of these lines are related to Beer's Law.

$$\text{Beer's Law} = \text{Absorbance} = \varepsilon bc \quad \text{(Equation 1)}$$

Where ε = molar absorptivity (L $mol^{-1}cm^{-1}$)
b = path length (cm)
c = concentration (mol L^{-1})

At a given temperature, each iron oxide has a specific molar absorptivity producing the following equation relating change in absorption and change in concentration.

$$\frac{A_{1260nm,t=0} - A_{1260nm,t=x}}{A_{450nm,t=0} - A_{450nm,t=x}} = \frac{\varepsilon_{magnetite} * b * (c_{magnetite(t=0)} - c_{magnetite(t=x)})}{\varepsilon_{maghemite} * b * (c_{maghemite(t=0)} - c_{maghemite(t=x)})} \quad \text{(Equation 2)}$$

The path lengths are equal. If the change in the concentrations of magnetite and maghemite are equal, as theoretically they should be assuming no further oxidation to hematite nor intermediates formed between magnetite and maghemite, then the slope of the relationship between the change in absorbance is equal to the ratio of molar absorptivities of magnetite to maghemite.

$$\frac{A_{1260nm,t=0} - A_{1260nm,t=x}}{A_{450nm,t=0} - A_{450nm,t=x}} = \frac{\varepsilon_{magnetite}}{\varepsilon_{maghemite}} \quad \text{(Equation 3)}$$

As shown in Figure 3-14 the different temperatures have different relationships. From the data, it can be seen that different temperatures have varying molar absorptivity ratios (Equation 3). These varying ratios again demonstrate that the molar absorptivity for magnetite and maghemite are dependent on the temperature at which they are measured. As the temperature of the measurements increase, the ratio of molar absorptivity of magnetite to maghemite increases. At 60 ^{o}C, the absorptivity for maghemite is higher than that of magnetite resulting in a shallow slope of 0.35. At 70 ^{o}C, the molar absorptivity for maghemite decreases, while the molar absorptivity of magnetite increases resulting in a steeper slope of 0.79. It is not until 80 ^{o}C that the molar absorptivity of magnetite becomes greater than that of maghemite, represented by a very steep molar absorptivity ratio/slope of 2.9. It should be remembered that the molar absorptivity of

magnetite is measured at 1260 nm which has been shown to have less absorption dependence on temperatures. Therefore, the major factor of molar absorptivity/slope change is due to the fluctuating molar absorptivity of maghemite. These trends are supportive of the fact that molar absorptivity of maghemite increases at lower temperatures and decreases for magnetite.

25 ^{o}C UV-Vis-NIR measurements. A set of oxidation experiments were conducted at temperatures of 60 and 80 ^{o}C; however, for these experiments the measurement temperature within the spectrometer was set at 25 ^{o}C. Figure 3-15 shows that when the measurement temperature was well below the experiment temperature, there is no difference from scan to scan. The lack of absorption change as well as the lack of a peak at 1260 nm indicates that the cold measurement temperature inhibits excitation of the Fe^{II}-Fe^{III} electron hoping transition. The overlapping of scans at 25 ^{o}C strengthens the argument that the absorption decay from one scan to the next at high measurement temperatures depicts the thermal charge transfer from the excited state to the ground state.

In Figure 3-16, which shows the oxidation of magnetite at 60 ^{o}C and 80 ^{o}C, it is shown that there is no increase in absorption in the UV-region as oxidation proceeds, which is why there is no isosbestic point. The cold measuring temperature possibly inhibited the excitations to a degree where they could not occur within the sample in the UV-region. It was stated earlier that low measurement temperatures amplify absorption in the UV-region; however, the drastic temperature change from oxidation to measurement could inhibit the light source energy from being absorbed by the electrons due to thermal convection losses within the sample.

The cold temperature readings inhibit accurate portrayals of the molar absorptivities of maghemite and magnetite by repressing transitions. By maintaining the temperature of oxidation with in the UV-Vis-NIR spectrometer, thermal energy is not lost; therefore, the energy that is added by the light source is used more efficiently for electron excitations.

Kinetics. The second scan was observed from sample to sample to avoid the use of the absorption peak that was only present in the first scan while still using a highly excited transition in the magnetite region. Again, Figure 3-12 shows that the kinetics of all the scans are quite similar and should not affect analysis.

Figures 3-17, 3-18, and 3-19 show the oxidation of magnetite using the second scan of the measurement period. Figure 3-20 monitors absorption at 1260 nm at all temperatures throughout oxidation to monitor magnetite. Figure 3-21 monitors absorption at 450 nm which is considered to be relative to the maghemite concentration. It is seen that the change in absorption is not linear. The rate of absorbance change is initially fast, but slows as oxidation proceeds. This observation supports the findings of Tang et al. who measured the diminishing Fe^{II} concentration over time and observed a change in rate that did not fit a simple rate reaction [6]. As Fe^{II} is oxidized at the surface of the magnetite, it forms a maghemite shell effectively insulating the magnetite from further Fe^{II} diffusion [4].

There is a much quicker decrease in absorption at 1260 nm at higher temperatures as shown in Figure 3-20. Increasing the temperature increases the rate at which Fe^{II} is diffused [6]. Temperature does not alter the activation energy for oxidation, but the activation energy is reached more easily at higher temperatures due to higher internal

energies. In the final samples, at 1260 nm there appears to be a common absorbance between all of the temperatures at the conclusion of their oxidation. The similar absorbance suggests that either there is no more magnetite present in the samples or at least an approximately similar degree of oxidation has been reached. This minimum absorption is slightly less than 0.9. At 450 nm (Figure 3-21), different absorptions were measured for the final samples, which is not due to the temperature of the oxidation but rather due to the temperature at which the samples were measured. It was discussed earlier that it is assumed that the higher absorption at 450 nm is due to the decrease in temperature which increased the molar absorptivity of maghemite in the UV-region. The concentration of maghemite is assumed to be very similar between the oxidation trials at different temperature; however, the rate at which these concentrations were reached was slower at lower temperatures.

Tang et al. conducted very similar oxidation experiments using nanoscale magnetite produced with TMAOH. During their oxidation trials, the black magnetite turned to an orange-red color and decreased in absorption in the near-IR region. Their oxidized particles were found to be maghemite by Raman spectroscopy and their magnetism. The absorption results also produce an isosbestic point near 400 nm. To measure the conversion of magnetite to maghemite, Tang et al. measured the changing concentration of Fe^{II}. It is noted that the reaction is fast at the beginning of oxidation; however, it becomes slow at the end signifying that the reaction does not fit simple rate laws. Tang et al. also found that reaction rate is high dependent on temperature. Higher temperatures increase the rate at which magnetite is oxidized. A plot was made relating

the amount of iron diffused over time, which was then used to calculate a diffusion coefficient.

$$\frac{M_t}{M_\infty}\times\frac{1}{t}=6\pi^{-1/2}\left(\frac{D}{a^2}\right)^{1/2}\times\frac{1}{t^{1/2}}-3\frac{D}{a^2} \quad \text{(Equation 4)}$$

Where M_t is the amount of iron that has oxidized over time t, M_∞ is the amount of iron that has diffused over infinite time, D is the diffusion coefficient, a is the radius, and t is time in minutes. When $\frac{M_t}{M_\infty}\times\frac{1}{t}$ is graphed versus $\frac{1}{t^{1/2}}$, the slope or the y-intercept is used to calculate a diffusion coefficient [6].

We tested to see if there is a correlation between our absorption data and their Fe^{II} diffusion data. By replacing the Fe diffusion variables with absorption variables plot was created; $\frac{Absorbance_{1260nmt=x}}{Absorbance_{1260nm\infty}}\times\frac{1}{t}$ versus $\frac{1}{t^{1/2}}$. Figure 3-21 shows that this relationship is linear as seen in the Tang et al. data. By making the same assumptions that Tang et al. made, diffusion coefficients can be calculated using the slope and y-intercept. The diffusion coefficients calculated are presented in Table 3-2 along with the diffusion coefficients calculated by Tang et al. It can be seen that there are very large discrepancies between the Tang et al. diffusion coefficients and the ones generated from our absorption data. The linear relationship of our absorptions is very clear in Figure 3-22; however, due to the poor diffusion coefficient correlation to Tang et al., it is assumed that Equation 4 does not present an accurate way of calculating accurate diffuse coefficients using absorption data.

Conclusions.

In conclusion, it is assumed that the decrease in absorption at 1260 nm over time is due to the loss of Fe^{II} in the octahedral coordination, lessening the electron hopping to Fe^{III} which creates the absorption band in the IR region. The increase in absorption at 450 nm over time is due to the increase in Fe^{III}-Fe^{III} transitions due to an increase in Fe^{III} from the oxidation of Fe^{II}. Temperature of oxidation greatly affects the rate at which oxidation occurs. Higher temperatures quickly oxidize magnetite, while a decrease of 10 ^{o}C, from 80 ^{o}C to 70^{o}C, will double the time required for the same degree of oxidation. A decrease in 20 ^{o}C, from 80 ^{o}C to 60 ^{o}C, will more than triple the oxidation time. Between the oxidation trials with different temperatures, a minimum magnetite absorption was reached, which helps draw the conclusion that equal degrees of oxidation occurred at each temperature However, even though maghemite concentrations should not have been significantly different from one trial to the next, the absorptions were much greater in the lower temperature trial. This is attributed to the fact that higher measurement temperatures negatively affect absorption by hindering the ferrimagnetism of maghemite partly caused by the magnetically coupled Fe^{III}-Fe^{III} transitions that create the band in the UV-region of the spectra.

References

1. Yean, S., et al., *Effect of magnetite particle size on adsorption and desorption of arsenite and arsenate.* Journal of Materials Research, 2005. **20**(12): p. 3255-3264.
2. Heathcock, A.M., *Characterization of Magnetite Nanoparticle Reactivity in the Presence of Carbon Tetrachloride*, in *Civil and Environmental Engineering*. 2006, Virginia Polytechnic and State University: Blacksburg. p. 50.
3. Sidhu, P.S., R.J. Gilkes, and A.M. Posner, *Mechanism of Low-Temperature Oxidation of Synthetic Magnetites.* Journal of Inorganic & Nuclear Chemistry, 1977. **39**(11): p. 1953-1958.
4. R.M. Cornell, U.S., *The Iron Oxides Structure, Properties, Reactions, Occurrences and Uses*. Second ed. 2003: Wiley-VCH Verlag GmbH & Co. KGaA, Weinheim. 664.
5. Vikesland, P.J., et al., *Particle size and aggregation effects on magnetite reactivity toward carbon tetrachloride.* Environmental Science & Technology, 2007. **41**(15): p. 5277-5283.
6. Tang, J., et al., *Magnetite Fe3O4 nanocrystals: Spectroscopic observation of aqueous oxidation kinetics.* Journal of Physical Chemistry B, 2003. **107**(30): p. 7501-7506.
7. Shebanova, O.N. and P. Lazor, *Raman study of magnetite (Fe3O4): laser-induced thermal effects and oxidation.* Journal of Raman Spectroscopy, 2003. **34**(11): p. 845-852.
8. Vayssieres, L., et al., *Size tailoring of magnetite particles formed by aqueous precipitation: An example of thermodynamic stability of nanometric oxide particles.* Journal of Colloid and Interface Science, 1998. **205**(2): p. 205-212.
9. Atkins, P.W., *Physical Chemistry*. Fourth Edition ed. 1990, New York: W. H. Freeman and Company. 995.
10. Sherman, D.M. and T.D. Waite, *Electronic-Spectra of Fe-3+ Oxides and Oxide Hydroxides in the near Ir to near Uv.* American Mineralogist, 1985. **70**(11-12): p. 1262-1269.
11. Leary, D.A.S.J.J., *Principles of Instrumental Analysis*. Fourth Edition ed, ed. M.M. Anderson. 1992, Orlando: Saunders College Publishing. 700.
12. Strens, R.G.J. and B.J. Wood, *Diffuse Reflectance Spectra and Optical-Properties of Some Iron and Titanium-Oxides and Oxyhydroxides.* Mineralogical Magazine, 1979. **43**(327): p. 347-354.
13. Fontijn, W.F.J., et al., *A consistent interpretation of the magneto-optical spectra of spinel type ferrites (invited).* Journal of Applied Physics, 1999. **85**(8): p. 5100-5105.

Tables and Figures

Table 3-1. Absorption summary for all temperatures.

Temperature	60 °C	70 °C	80 °C
450 nm $_{t=0}$	3.843	3.556	3.646
450 nm $_{t=final}$	4.753	4.023	3.792
1260 nm $_{t=0}$	1.309	1.326	1.335
1260 nm $_{t=final}$	.888	.842	.884
Isosbestic point	560 nm	545 nm	490 nm

Table 3-2. Diffusion Coefficients oxidation of magnetite. *Da* coefficient is derived from the slope of the graph in Figure 3-21. *Db* is the coeffiecnt derived from the y-intercept.

Absorption Coefficients			
T (C)	**60 °C**	**70 °C**	**80 °C**
Da (cm^2/s)	974246	2400949	4556777
Db (cm^2/s)	627750	1417500	2693250
Percent difference	35.56	40.96	40.89
Fe Diffusion Coefficient (Tang et al.)			
T (C)	**60 °C**	**70 °C**	**80 °C**
Da (cm^2/s)	64.90437	195.765	595
Db (cm^2/s)	63.25485	179.1407	561
percent difference	2.54	8.49	5.71

Figure 3-1. Oxidation setup. Photograph by John Templeton.

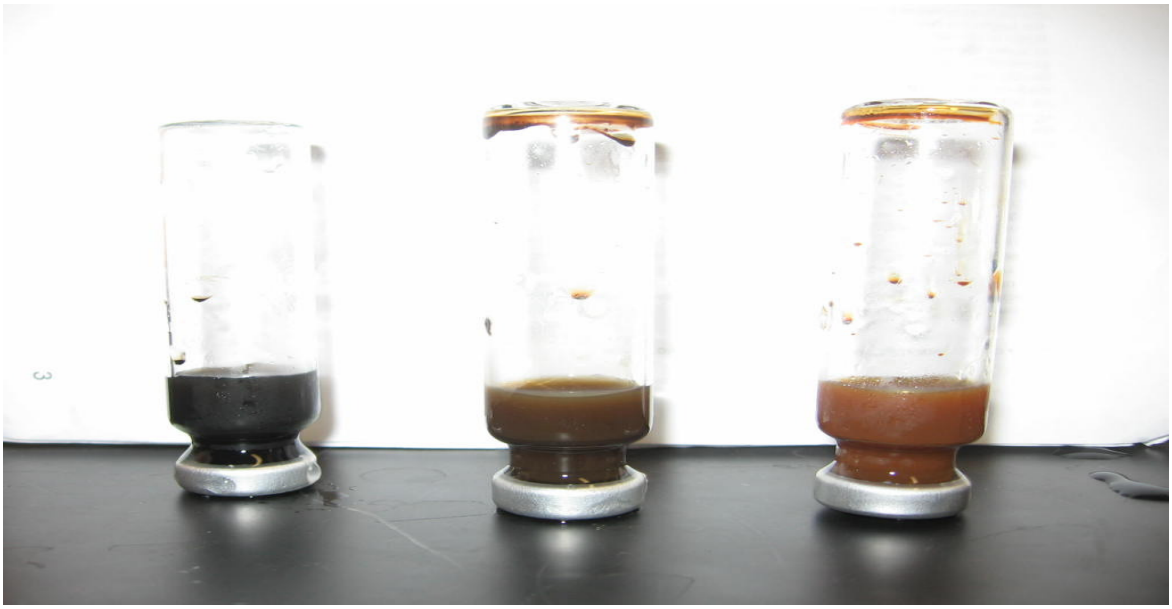

Figure 3-2. Magnetite oxidation samples. In order from left to right, magnetite at t = 0, t = 3 hours of oxidation, and t = 10 hours of oxidation. Photograph by John Templeton.

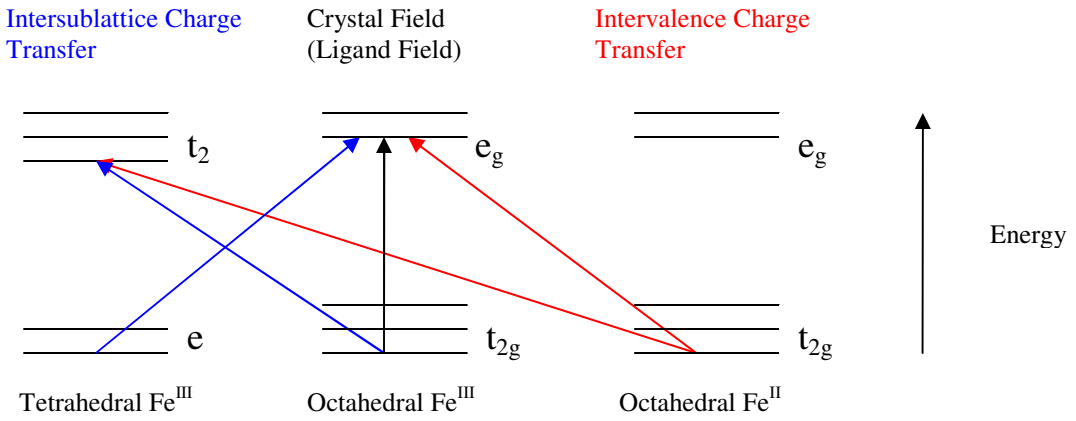

Figure 3-3. Non-identical *d* orbitals transitions of octahedral and tetrahedral iron and their energy levels.

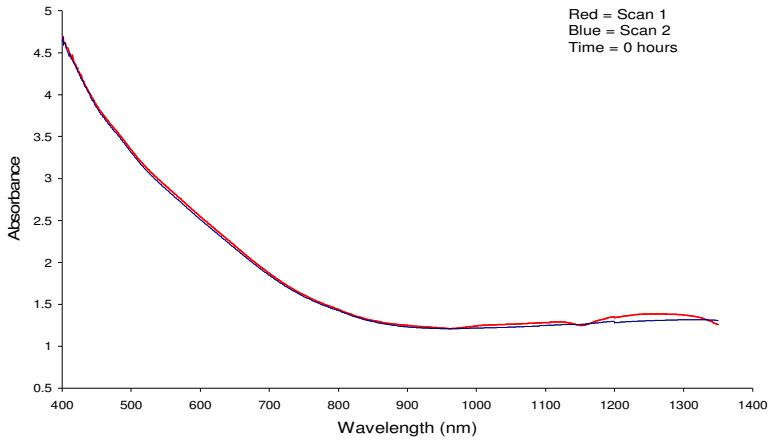

a)

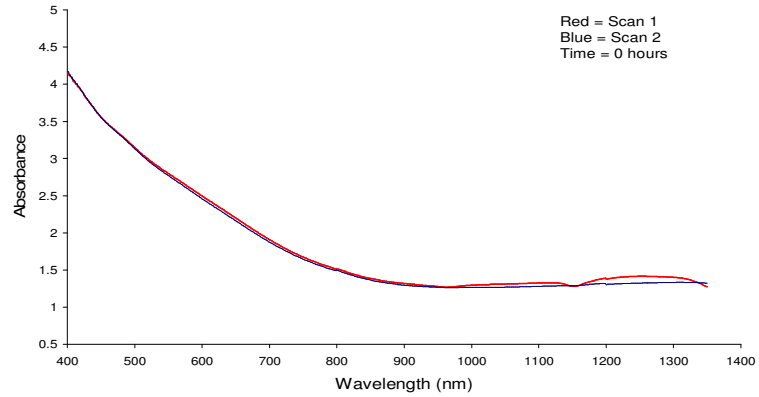

b)

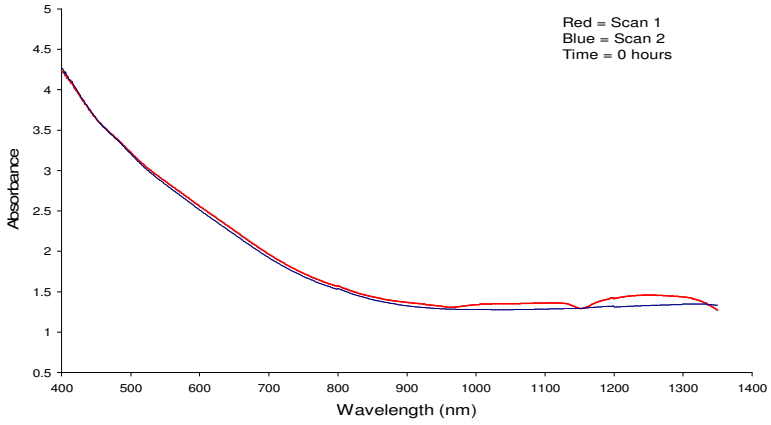

c)

Figure 3-4. First and second scans at initiation (t = 0) of oxidation. a) 60 ^{o}C, b) 70 ^{o}C c) 80 ^{o}C.

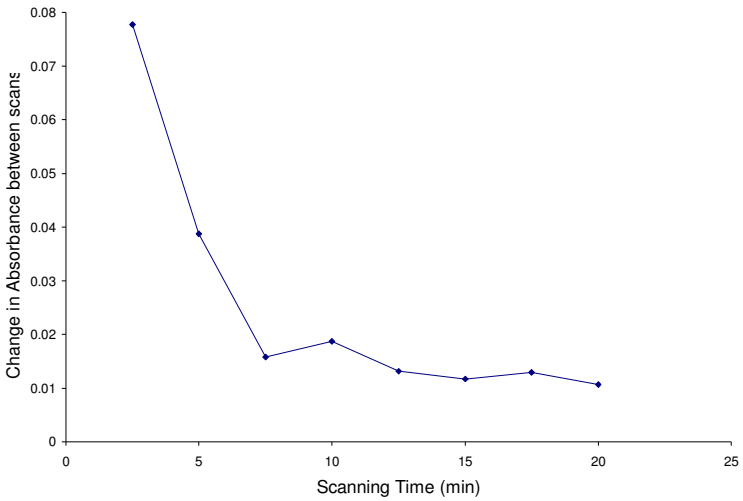

a)

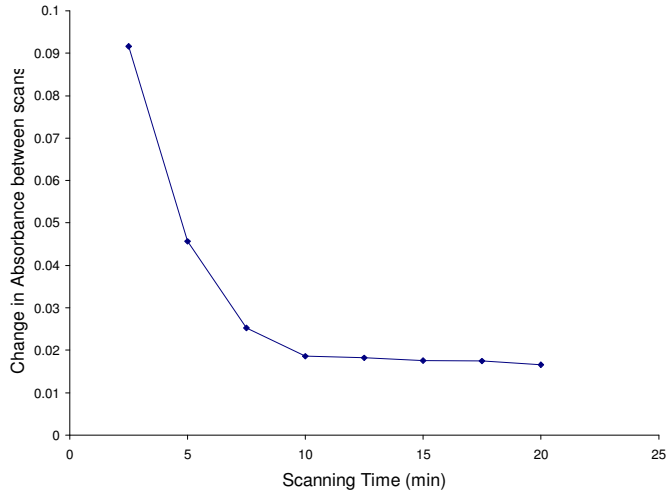

b)

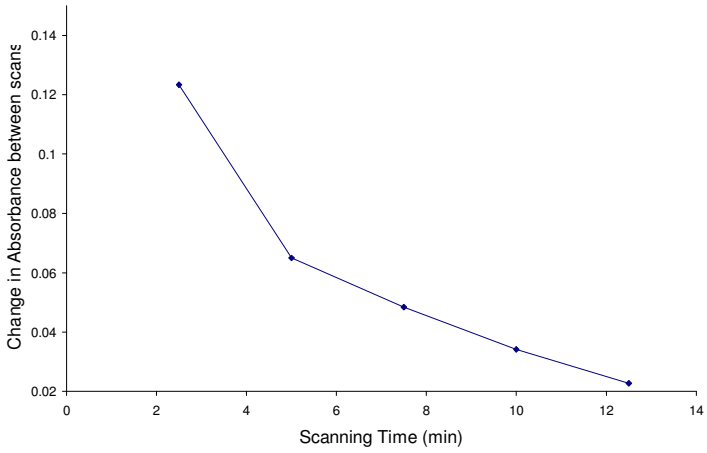

c)

Figure 3-5. The change in absorption through the measurement period at t = 0, each point representing a separate scan for a) 60^{o}C, b) 70 ^{o}C, and c) 80 ^{o}C. The straight lines represent the possible trend between points.

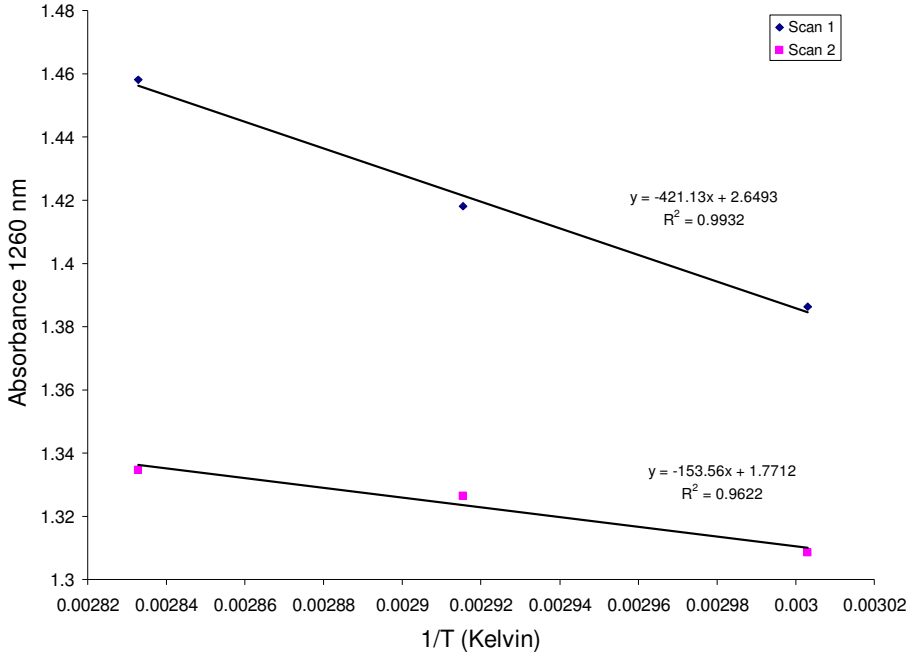

a)

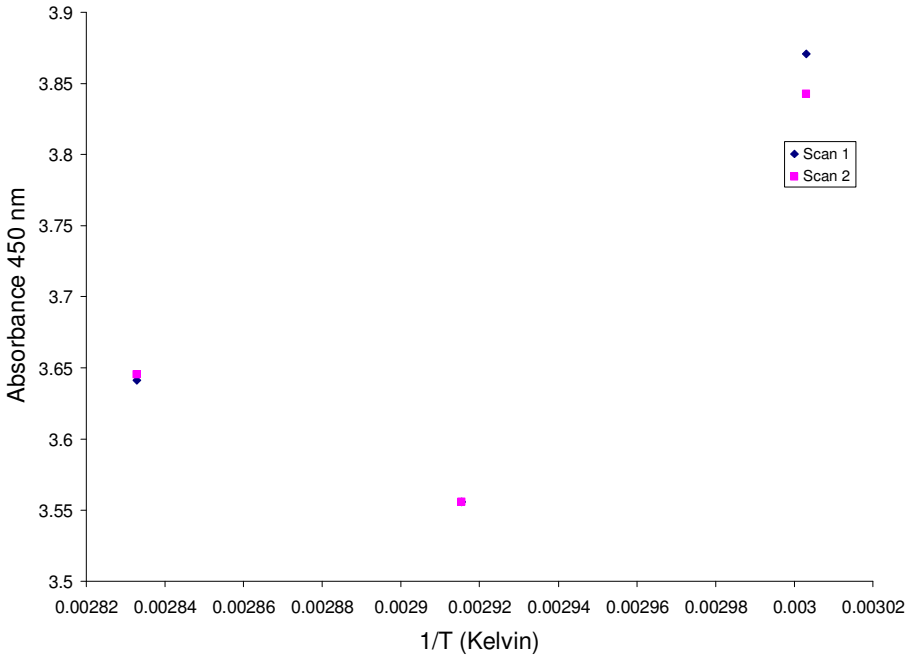

b)

Figure 3-6. The effect of temperature on the first and second scan absorptions at a)1260 nm and b) 450 nm at initiation of oxidation (t = 0).

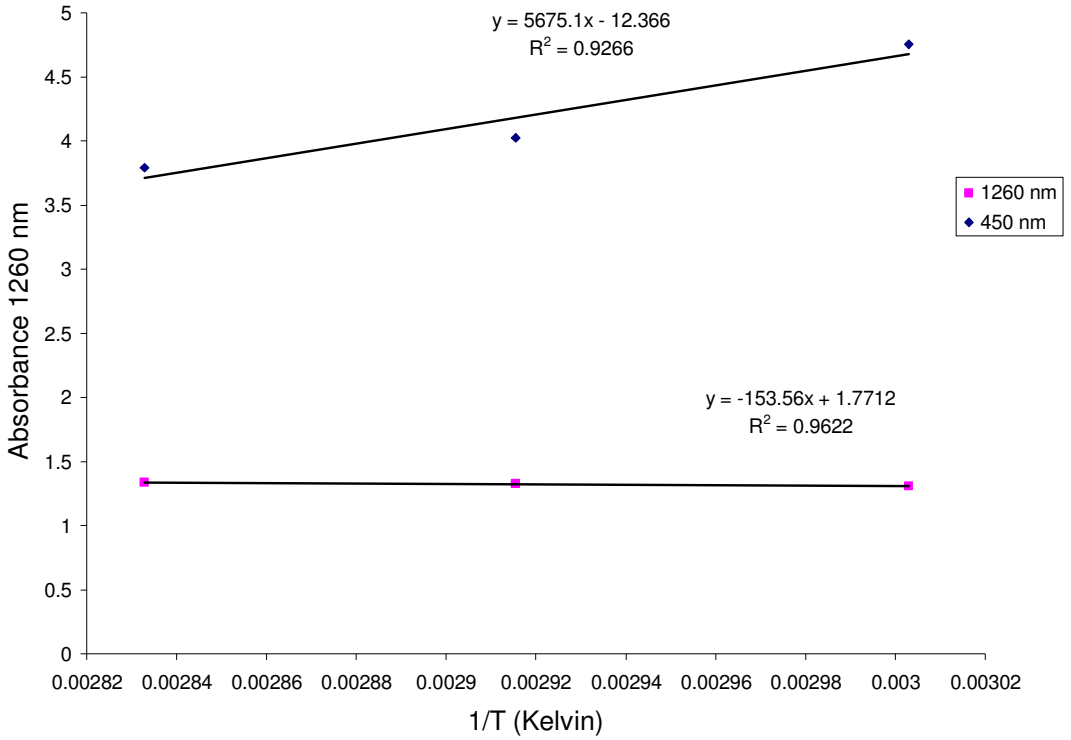

Figure 3-7. The effect of temperature on the transitions. At t=0 the Fe^{II}-Fe^{III} electron hopping is at its greatest (1260 nm). At t=final, the Fe^{III}-Fe^{III} transition is at its greatest (450nm).

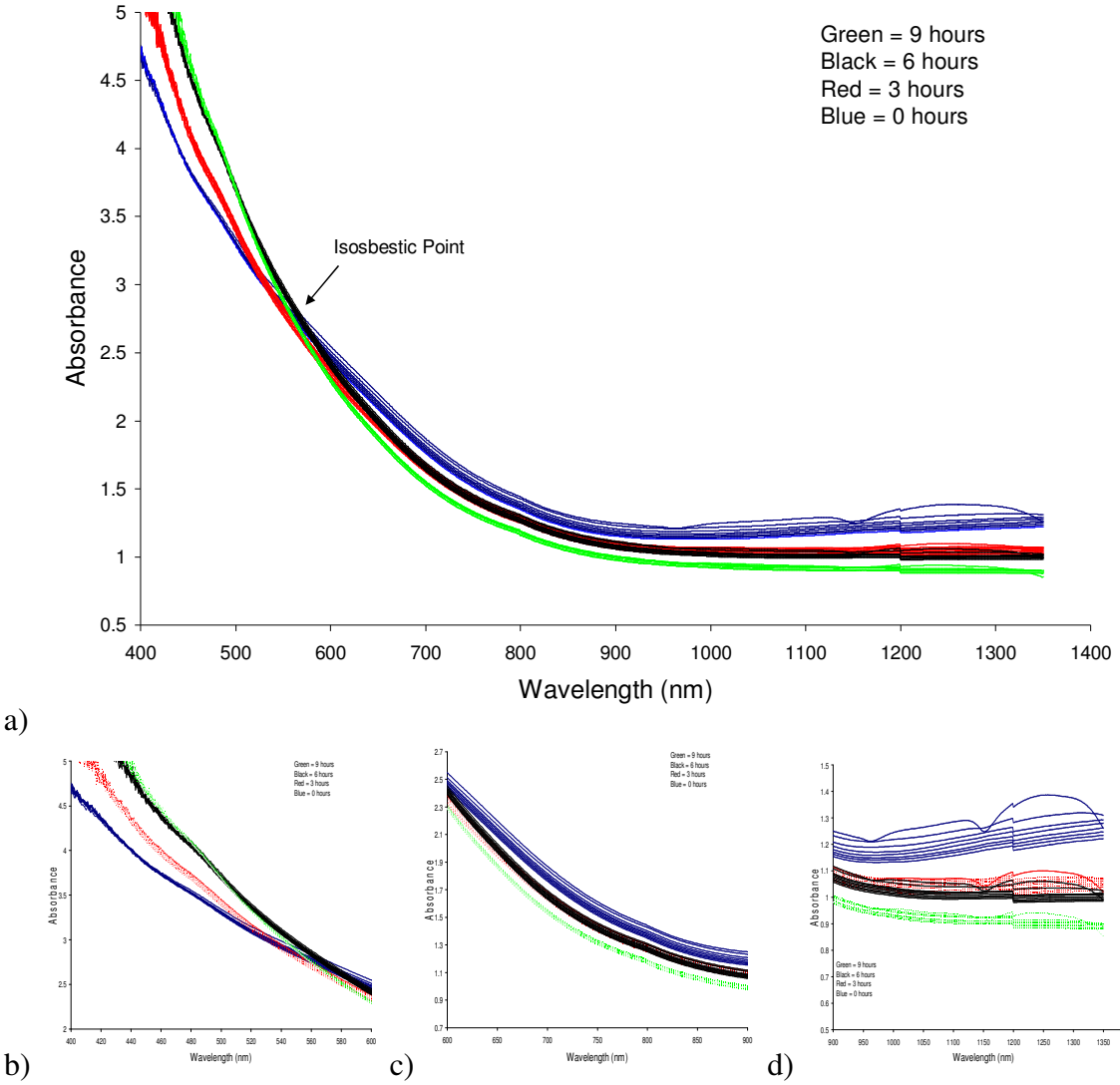

Figure 3-8. a) Oxidation of magnetite at 60 ^{o}C measured by UV-VIS-NIR spectroscopy. b) The Fe^{III}-Fe^{III} transition absorption region (to the left of the isosbestic point at 560 nm). c) The middle range spectra of the measurements. d) Fe^{II}-Fe^{III} transition region of absorption. In c) and d), the top absorption of each color represents the first scan, followed by, in sequential order, the remaining scans of the sample. Each color depicts a specific time and all of the scans performed on that sample.

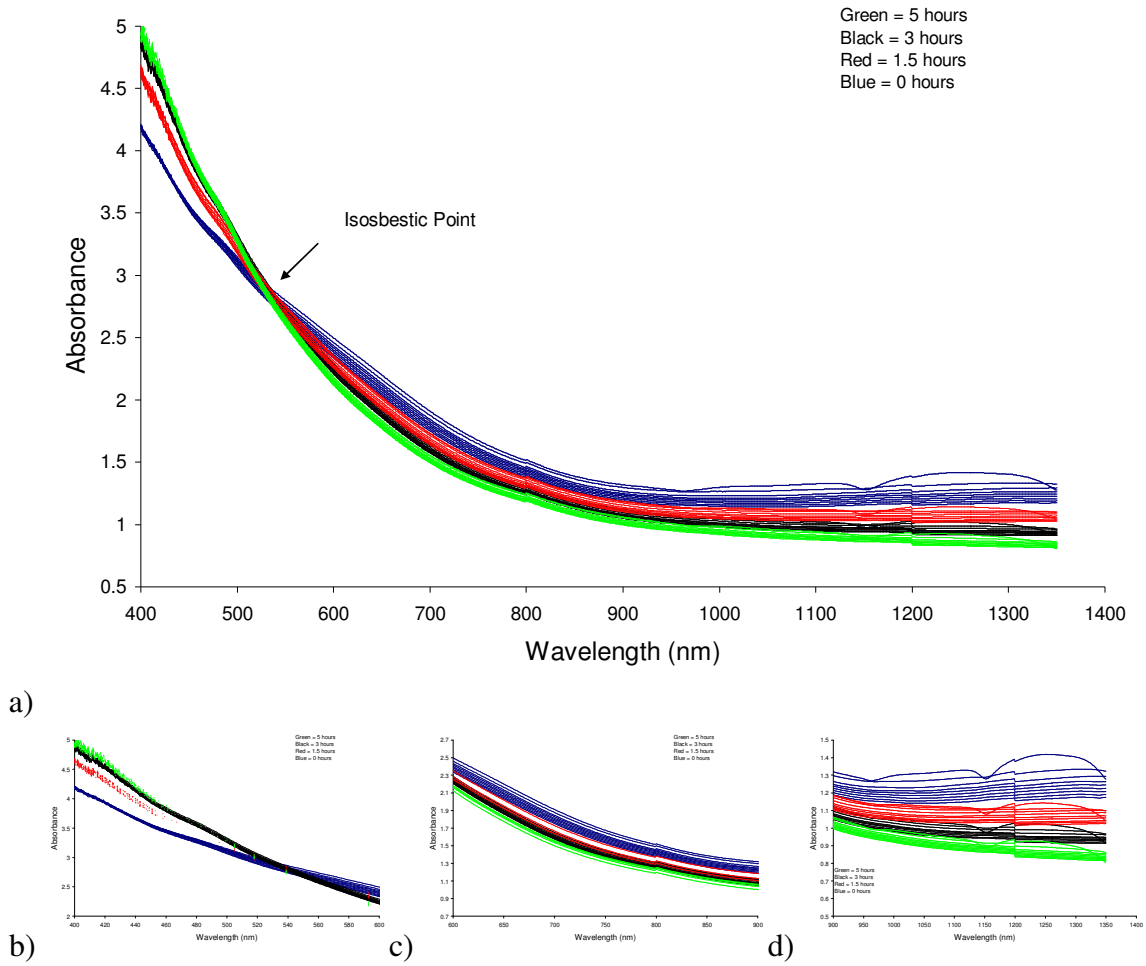

a)

b) c) d)

Figure 3-9. a) Oxidation of magnetite at 70 ^{o}C measured by UV-VIS-NIR spectroscopy. b) The Fe^{III}-Fe^{III} transition absorption region (to the left of the isosbestic point at 545 nm). c) The middle range spectra of the measurements. d) Fe^{II}-Fe^{III} transition region of absorption. In c) and d), the top absorption of each color represents the first scan, followed by, in sequential order, the remaining scans of the sample. Each color depicts a specific time and all of the scans performed on that sample.

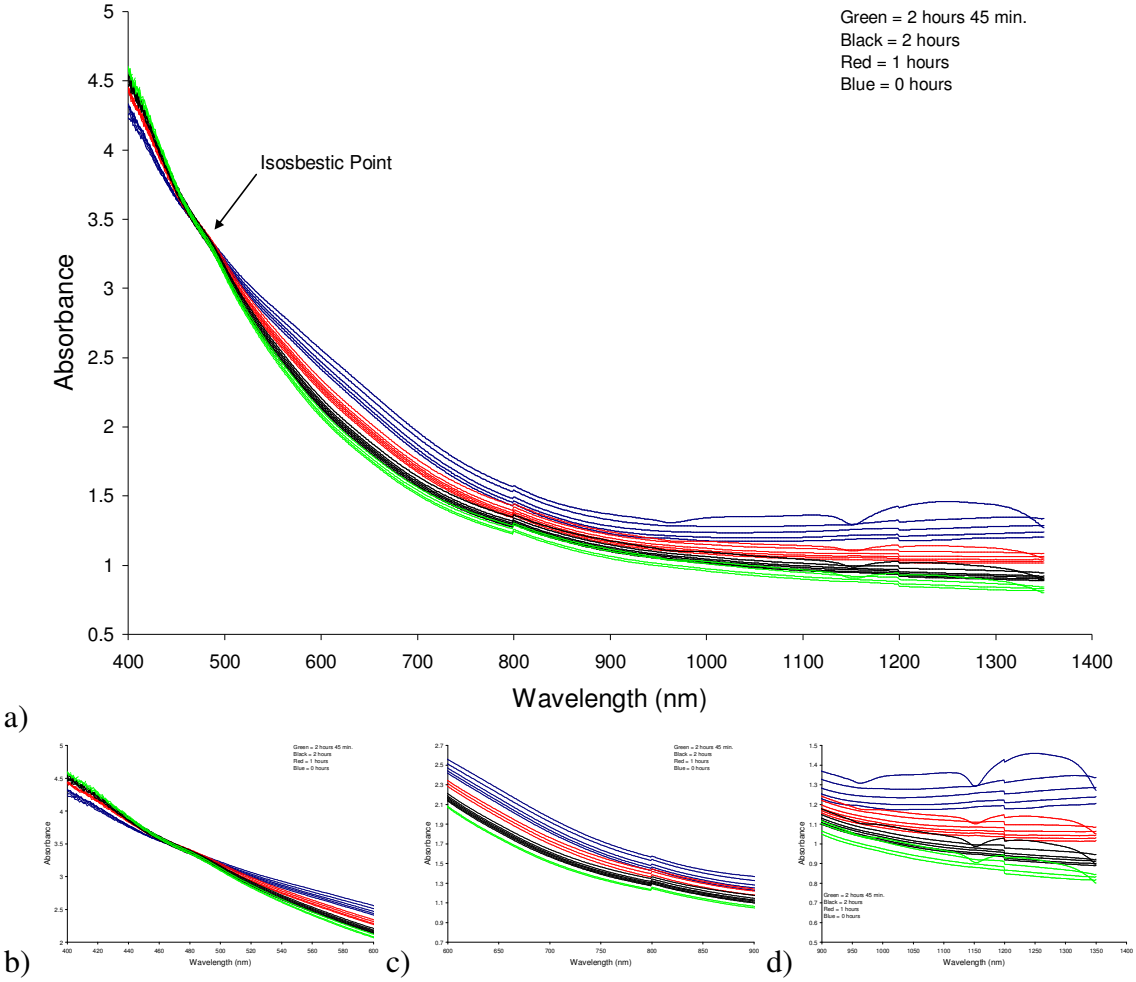

Figure 3-10. a) Oxidation of magnetite at 80 ^{o}C measured by UV-VIS-NIR spectroscopy. b) The Fe^{III}-Fe^{III} transition absorption region (to the left of the isosbestic point at 490 nm). c) The middle range spectra of the measurements. d) Fe^{II}-Fe^{III} transition region of absorption. In c) and d), the top absorption of each color represents the first scan, followed by, in sequential order, the remaining scans of the sample. Each color depicts a specific time and all of the scans performed on that sample.

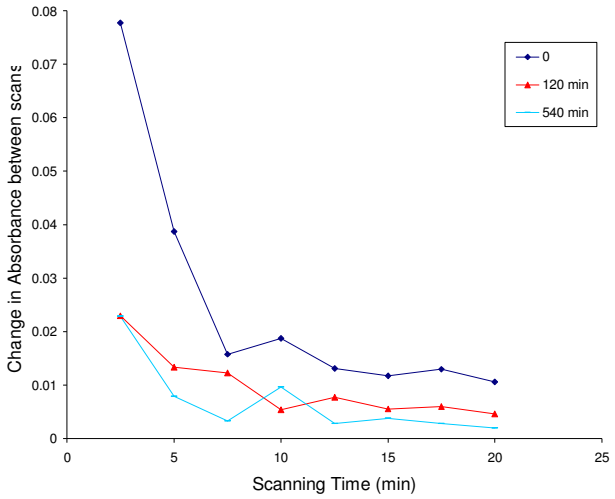

a)

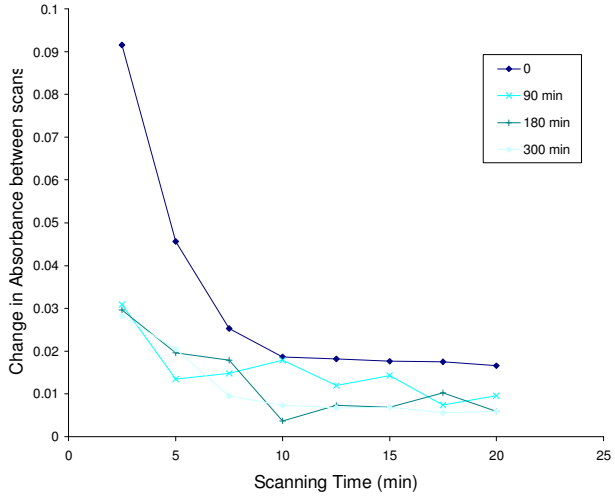

b)

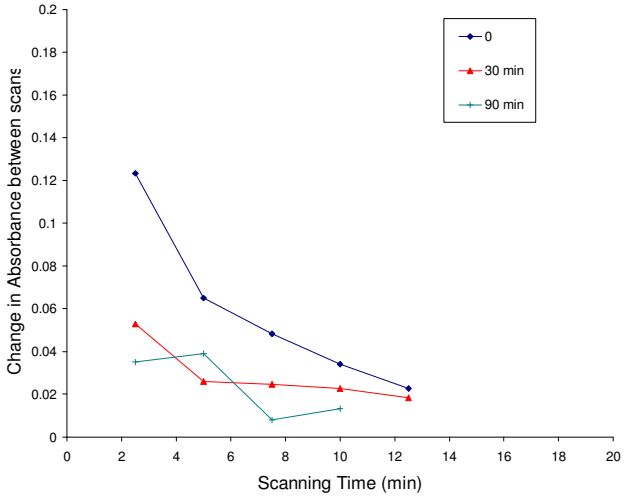

c)

Figure 3-11. The effect of sequential scans on absorption at 1260 nm for a) 60 ^{o}C, b) 70 ^{o}C, and c) 80 ^{o}C. Each point represents a separate scan and the lines represent possible trends between the points.

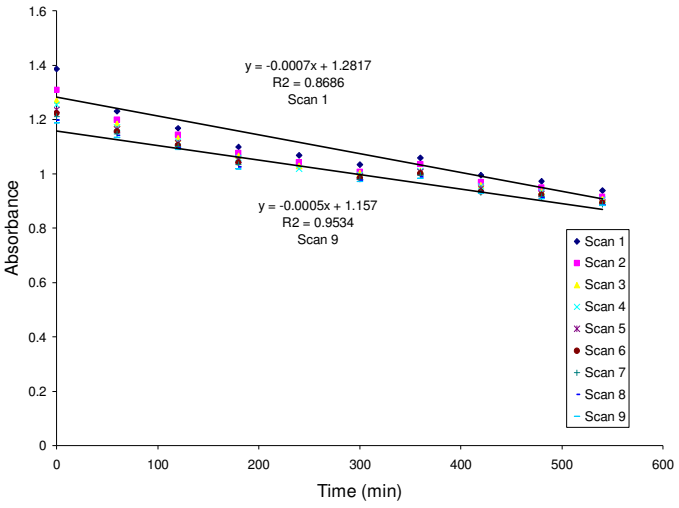

a)

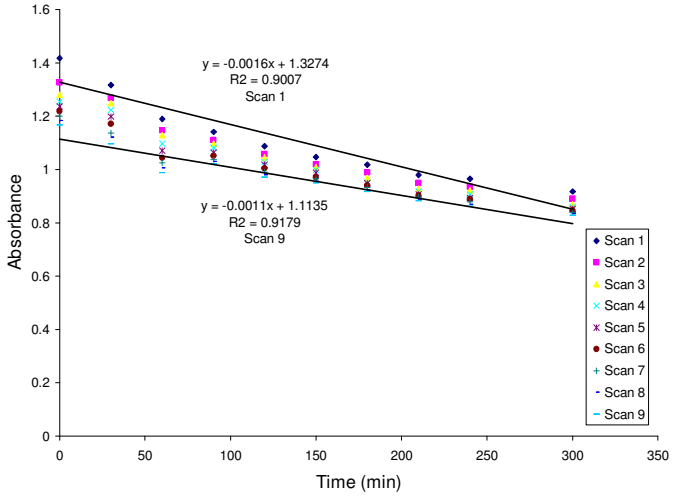

b)

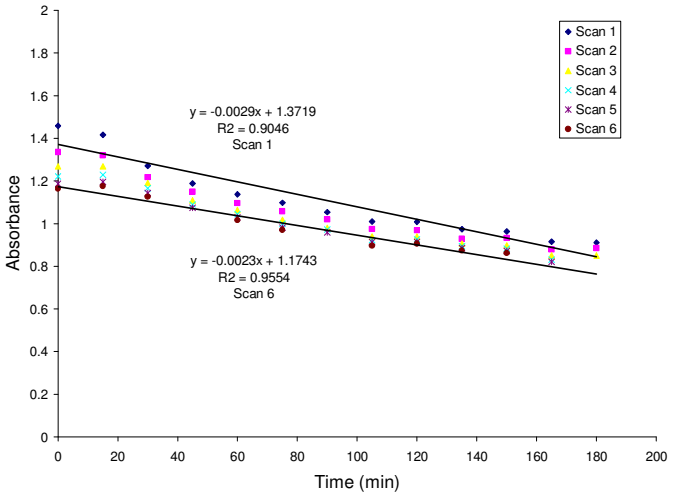

c)

Figure 3-12. The effect of different scans on the kinetics of oxidation. The trend was made by measuring the absorption at 1260 nm. a) 60 ^{o}C, b) 70 ^{o}C, c) 80 ^{o}C. The time between scans is approximately 2 minutes.

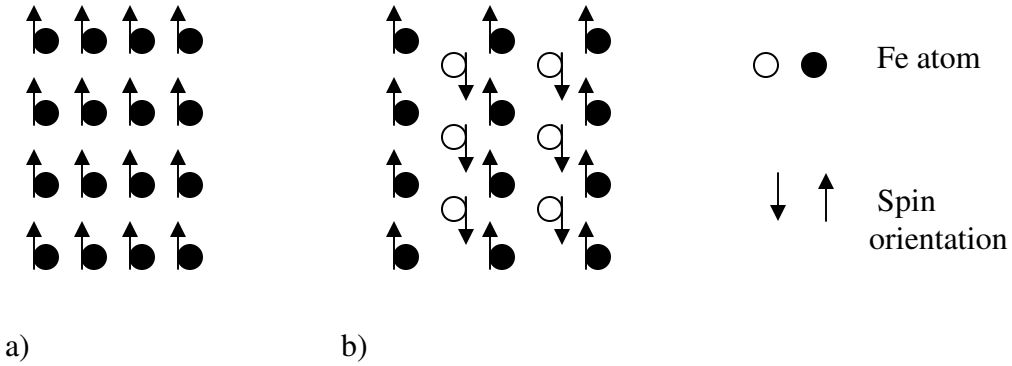

Figure 3-13. Arrangement of a) ferromagnetism and b) ferrimagnetism.

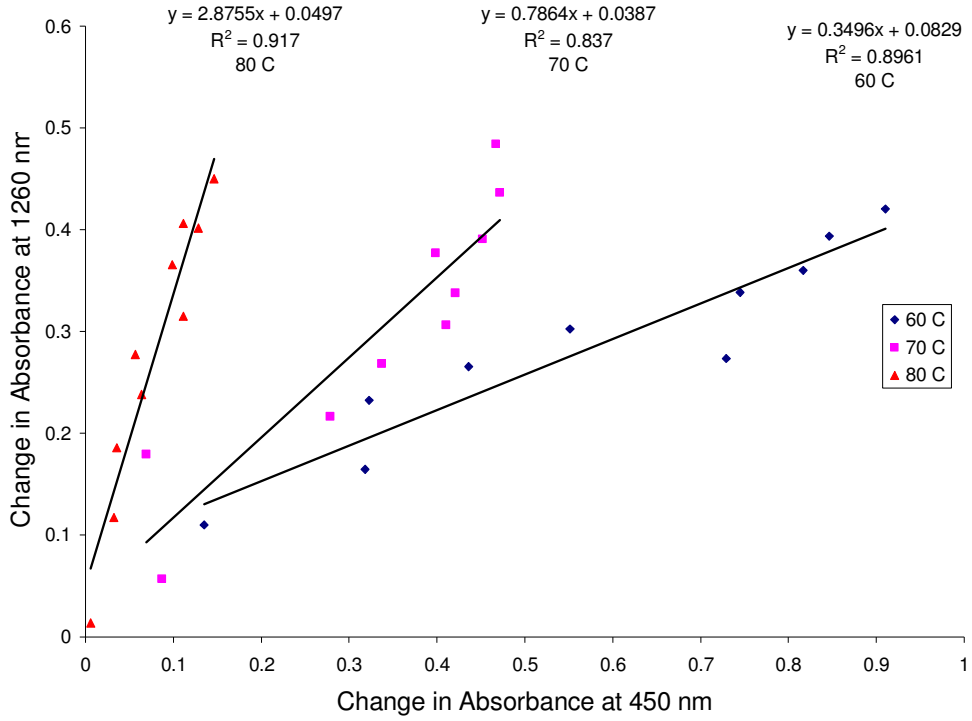

Figure 3-14. Beer's Law related to the change in absorption at 1260 nm and 450 nm.

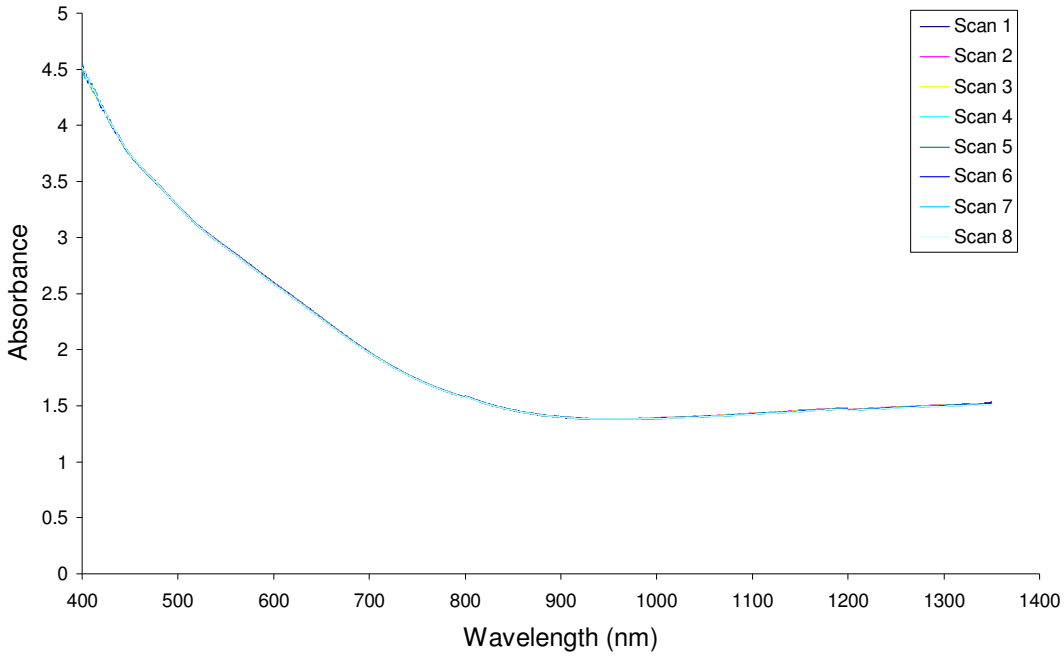

a)

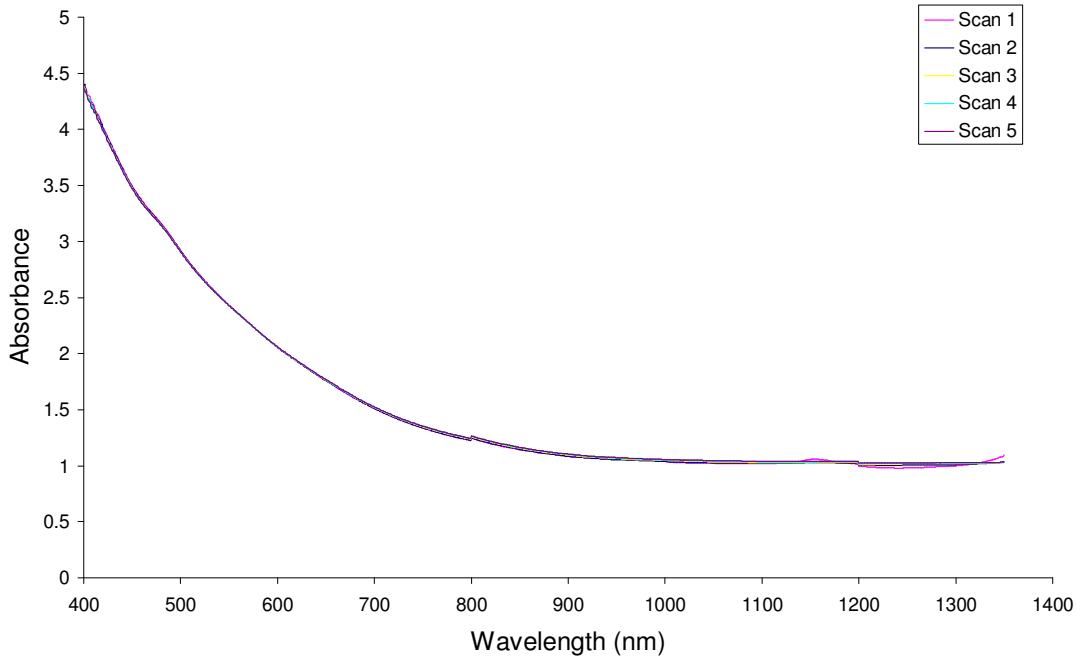

b)

Figure 3-15. The effect of sequential scans on absorption within the same sample at a measuring temperature of 25°C at oxidation trials of a) 60 °C and b) 80 °C.

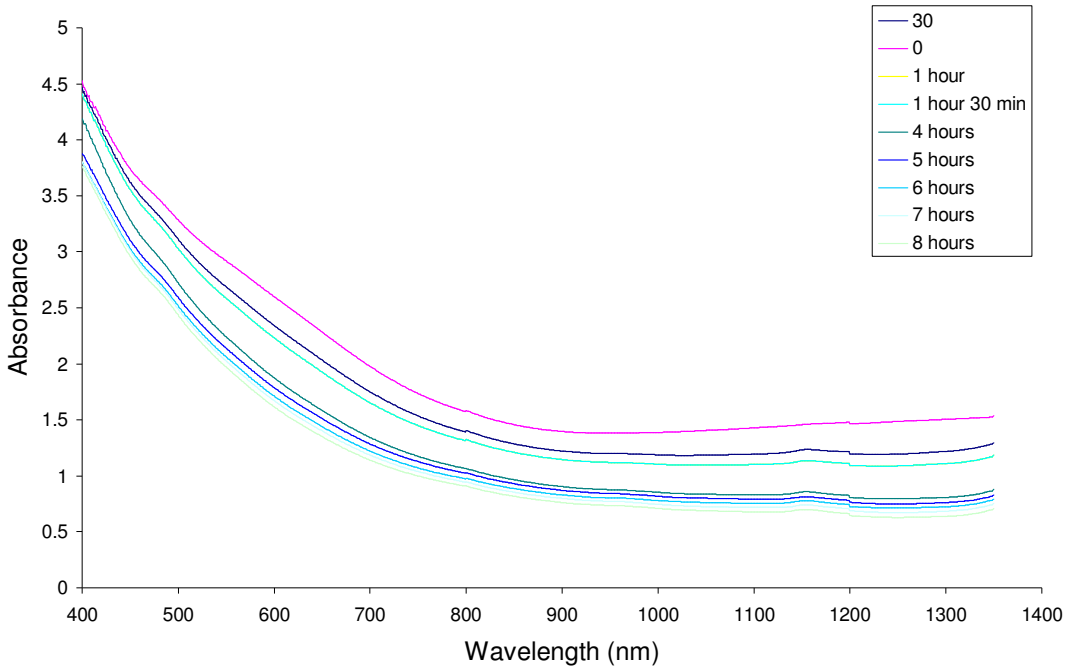

a)

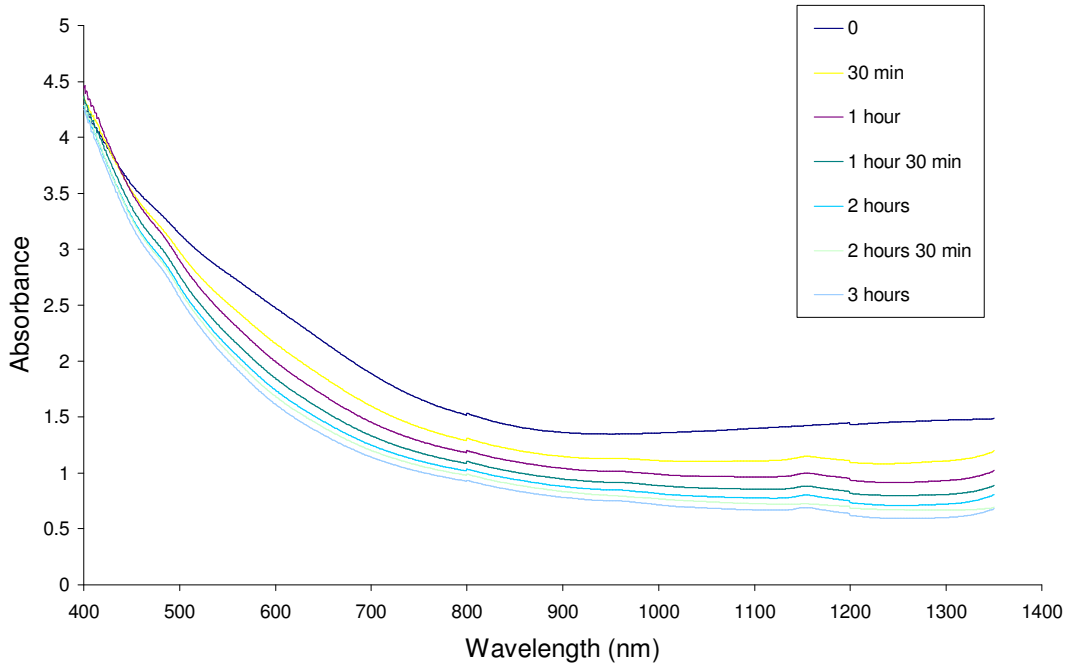

b)

Figure 3-16. UV-Vis-NIR spectroscopy analysis with temperature measurements set at 25^{o}C, scan 1, for oxidations at a) 60 ^{o}C and b) 80 ^{o}C.

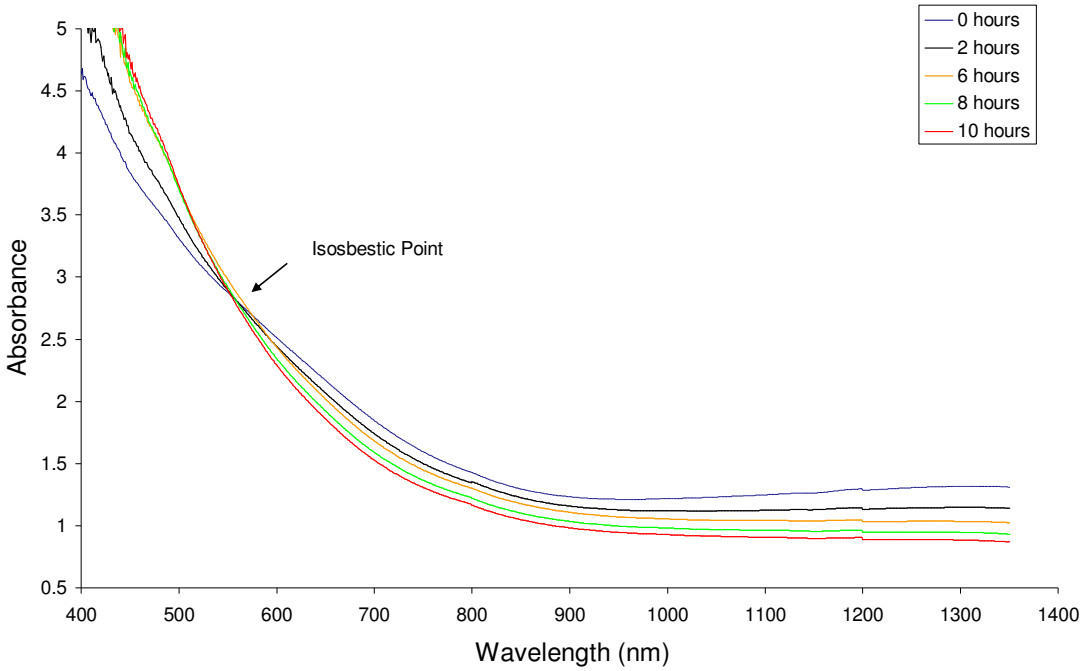

a)

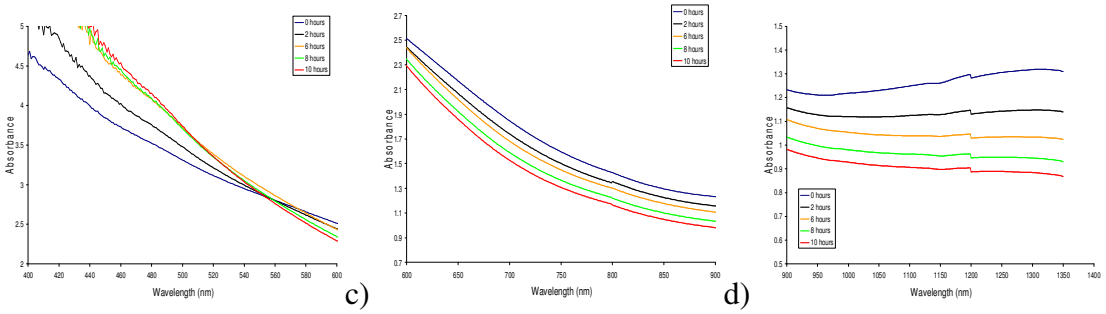

b) c) d)

Figure 3-17. a) Oxidation of magnetite using the second scan from the measuring period at 60 ^{o}C by UV-VIS-NIR spectroscopy. b) The Fe^{III}-Fe^{III} transition absorption region (to the left of the isosbestic point at 560 nm). c) The middle range spectra of the measurements. d) Fe^{II}-Fe^{III} transition region of absorption.

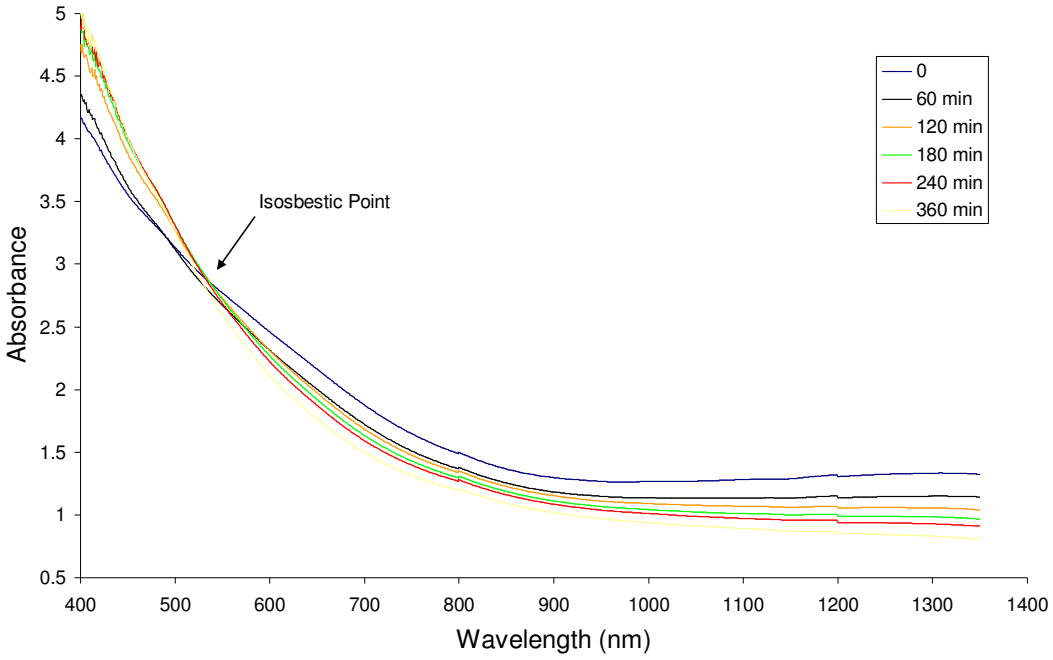

a)

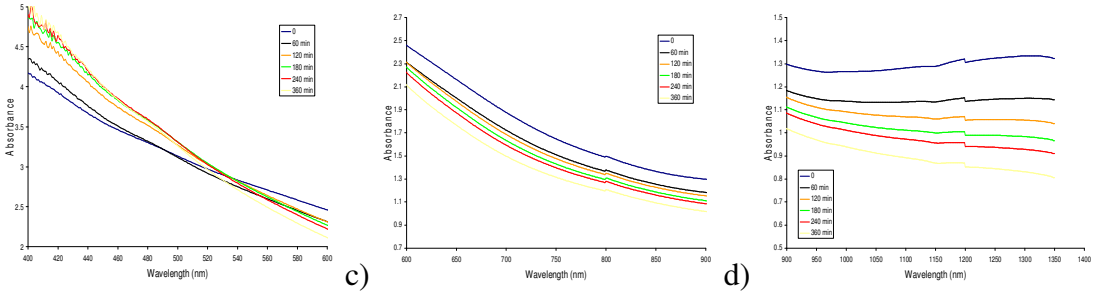

b) c) d)

Figure 3-18. a) Oxidation of magnetite using the second scan from the measuring period at 70 ^{o}C by UV-VIS-NIR spectroscopy. b) The Fe^{III}-Fe^{III} transition absorption region (to the left of the isosbestic point at 545 nm). c) The middle range spectra of the measurements. d) Fe^{II}-Fe^{III} transition region of absorption.

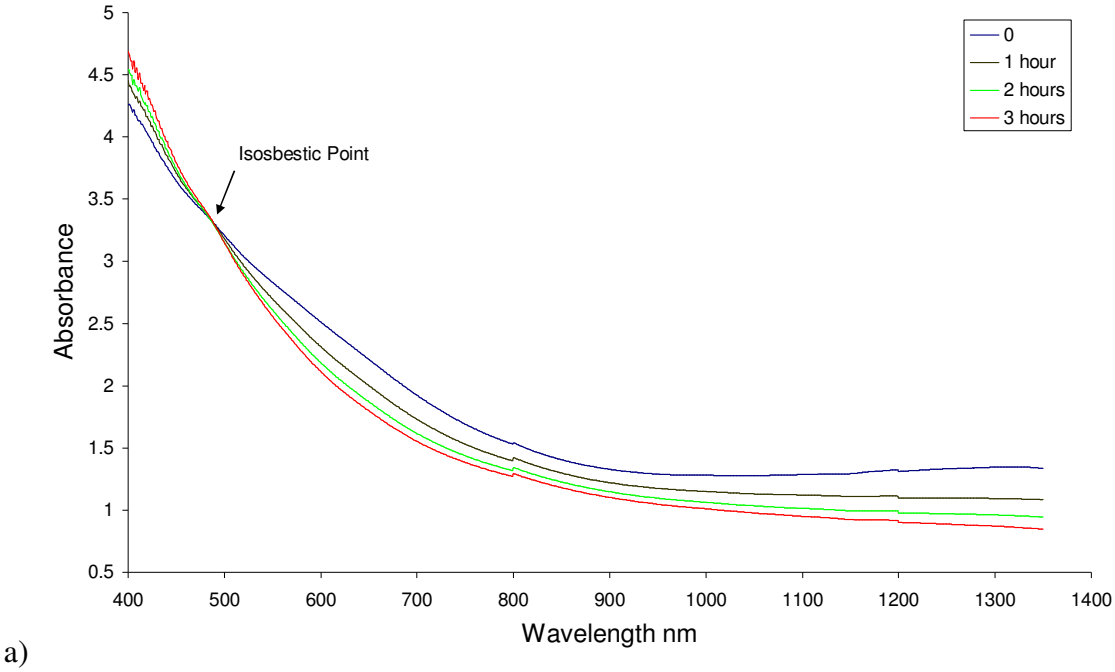

a)

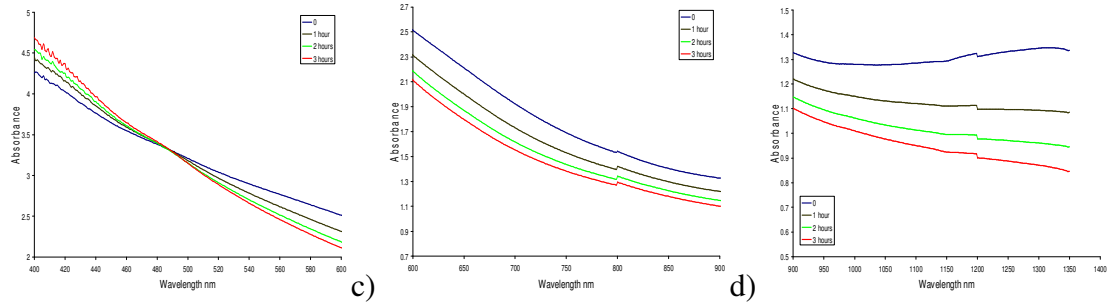

b) c) d)

Figure 3-19. a) Oxidation of magnetite using the second scan from the measuring period at 80 ^{o}C by UV-VIS-NIR spectroscopy. b) The Fe^{III}-Fe^{III} transition absorption region (to the left of the isosbestic point at 490 nm). c) The middle range spectra of the measurements. d) Fe^{II}-Fe^{III} transition region of absorption.

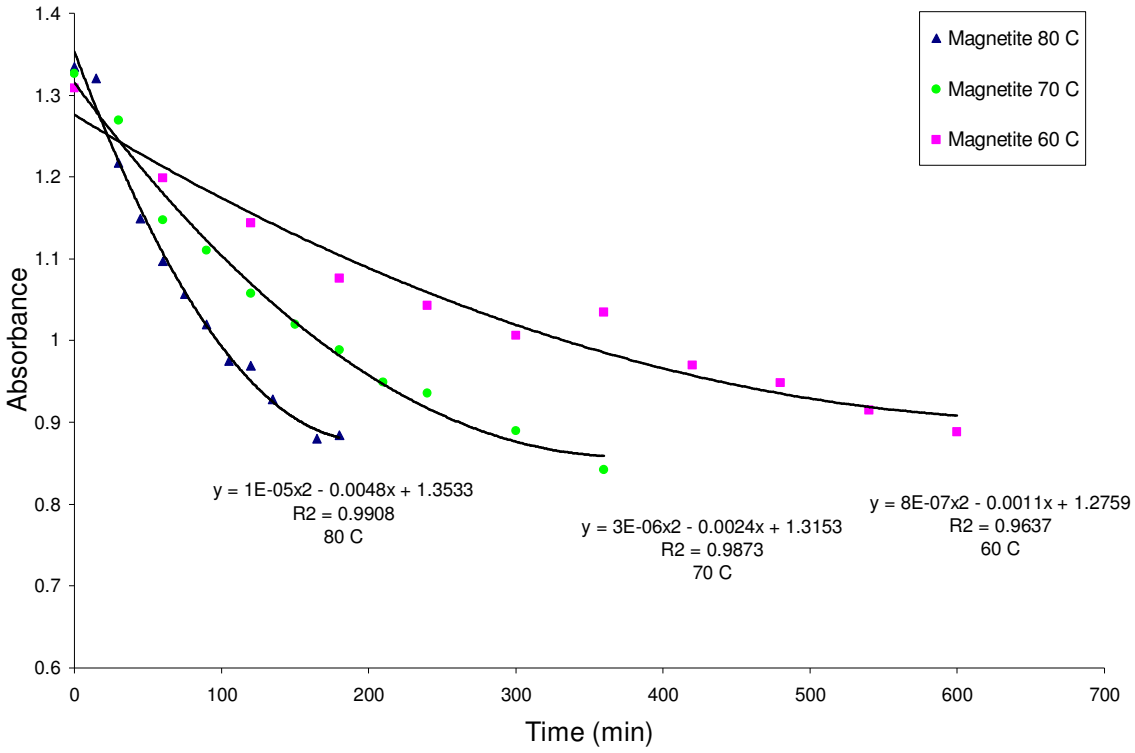

Figure 3-20. The absorption at 1260 nm in the Fe^{II}-Fe^{III} transition region throughout oxidation.

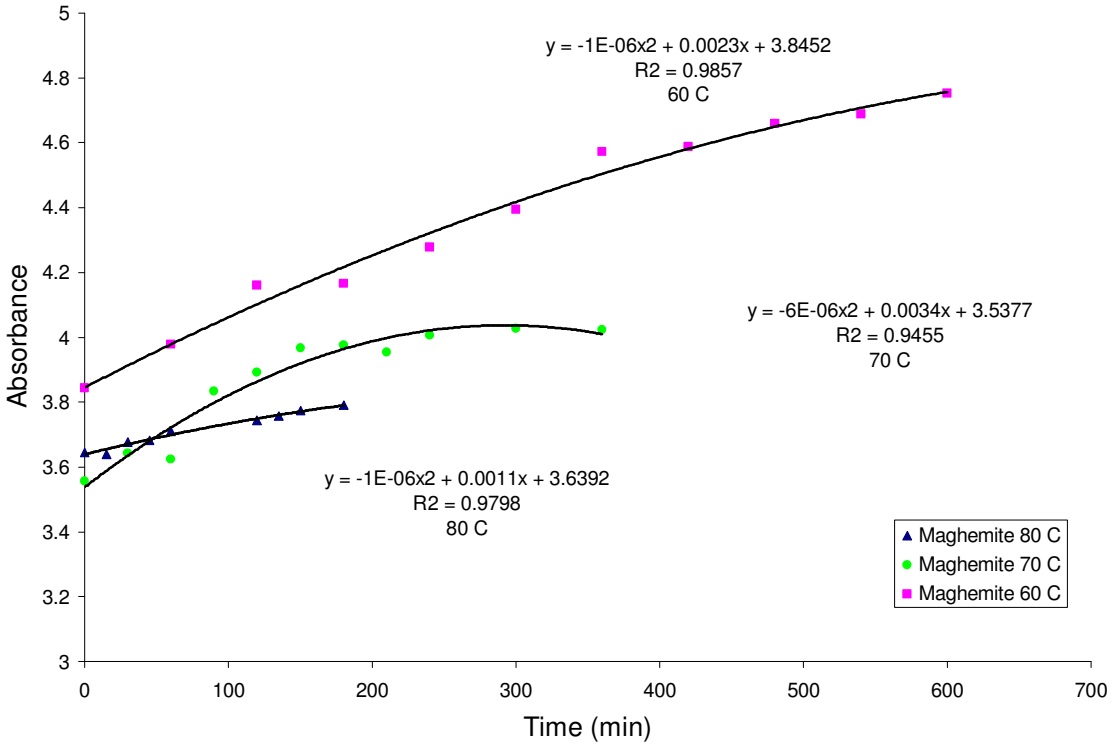

Figure 3-21. The absorption at 450 nm in the Fe^{III}-Fe^{III} transition region throughout oxidation.

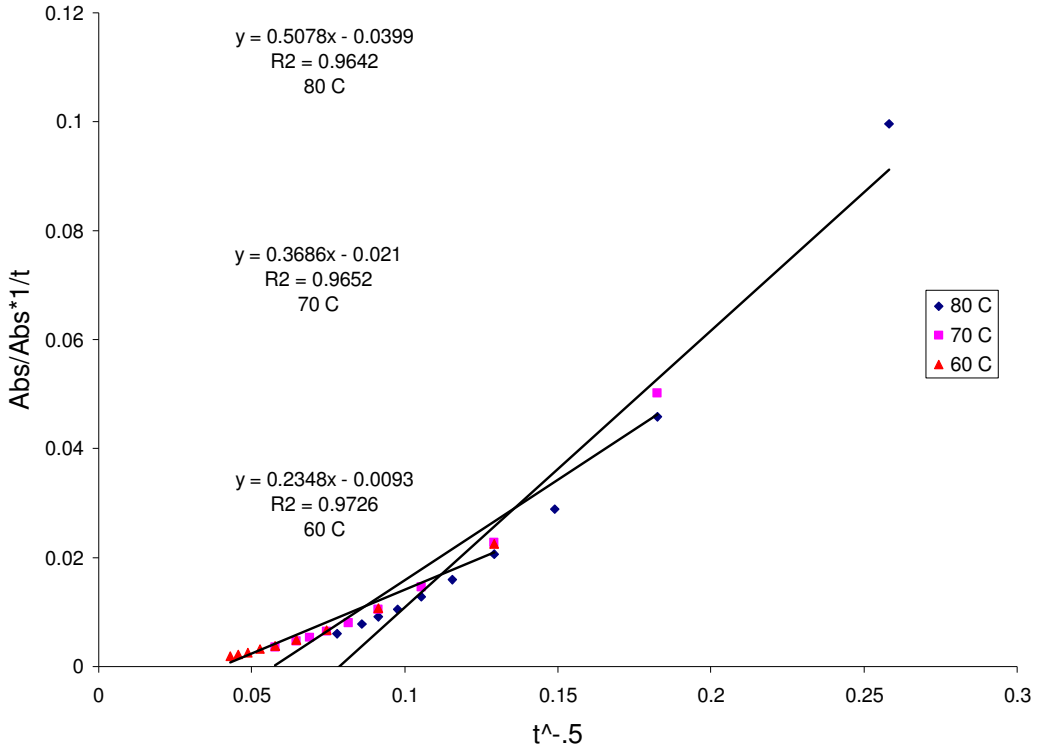

Figure 3-22. $\frac{Absorbance_{1260nmt=x}}{Absorbance_{1260nm\infty}} \times \frac{1}{t}$ versus $\frac{1}{t^{1/2}}$ plot. The slope and y-intercept were used to calculate a diffusion coefficient for each temperature.

IV. Magnetite Oxidation and Arsenic Adsorption

Introduction

Iron oxides, including magnetite, are found all over the world. Their abundance has lead to the study of their natural uses within the environment as well as their possible uses by mankind [1]. Magnetite, a composite of trivalent and divalent iron, has many properties of great interest to engineering. Magnetism and surface reactivity warrant much investigation for groundwater system remediation [2, 3]. The properties of magnetite are altered during oxidation, which transforms magnetite into maghemite, and through further oxidation to hematite. There have been many studies that have identified the different iron oxides by use of Raman spectroscopy [1, 4, 5]. Raman spectroscopy identifies chemical bonds within a sample by measuring energy shifts caused by the scattering of a laser. Although many studies use Raman spectroscopy to identify iron oxides, little work has been done to monitor the oxidation of magnetite to other iron oxides.

Arsenic contaminated groundwater systems can be found throughout the world [6]. The most common oxidation state naturally found, arsenic (III), is also the most dangerous to human health. Current methods of arsenic extraction from drinking water and groundwater systems, such as reverse osmosis and membrane filtration, are expensive and impractical for developing countries [6]. Research is currently being conducted to investigate arsenic adsorption characteristics to iron oxides, including magnetite [2, 6]. Nanoscale magnetite and their magnetic properties have peaked the interest of *in situ* remediation [2, 7]. Trivalent arsenic (As^{III}), in an aqueous medium, is dominantly present as the neutral species, $H_3AsO_3^0$ [6]. The neutrality of the species

allows the arsenic to avoid electrostatic forces due to the surface charge of magnetite. Through ligand exchange, the arsenic binds to the magnetite surface as a bidentate-binuclear complex [6]. Studies have shown that as surface area increases the capacity for arsenic adsorption increases [6]. Other determinants of arsenic adsorption, as investigated by this study, are the pH and the ionic strength of the suspension.

Materials and Methods

De-aerated water was used for the synthesis of magnetite and for all experiments. Deionized water (>18.1 MΩ) from a Barnstead Nanopure filtration system was boiled for approximately 50 minutes; halfway through this period the water was sparged with argon gas while continuing to boil. The de-aerated water was capped, cooled, and stored within an anaerobic glovebox (Coy Laboratory Products Inc.) until it was used. All chemicals employed were reagent grade from Fisher Scientific, Sigma-Aldrich, or Arcos Organics.

Particle Synthesis. Magnetite was synthesized in an anaerobic glovebox with an atmospheric composition of 95%/5% N_2/H_2. Particles were prepared by a method established by Vayssieres et al. involving the co-precipitation of divalent iron (Fe^{II}) and trivalent iron (Fe^{III}) [8]. In brief, a base solution of 1 M sodium hydroxide and 1 M sodium chloride was continually stirred, while an iron solution was added dropwise. The iron solution was comprised of 0.1 M ferrous chloride mixed with an equal volume of 0.2 M ferric chloride. All chemicals were weighed outside of the anaerobic chamber, but the final solutions were prepared within the chamber using de-aerated water. The volumetric ratio of iron to base was held at 3:2 with a pH value above 12. Throughout the addition of the iron to the base, an overhead mixer, stirring rod and PTFE stirring blade rapidly mixed the suspension. Upon completion of the magnetite synthesis, the particles were

separated from the background solution using a magnet. The supernatant was decanted and repeatedly replaced with de-aerated water to remove excess salts. The washed magnetite particles were stored in the anaerobic chamber in a polypropylene container in de-aerated water at a pH of approximately 10.

The mass concentrations of the magnetite solutions were determined by drying a specific volume aliquot of the well mixed suspension in an oven at 75 ^{o}C. The mass of the dry iron oxide along with the known sample volume enabled calculation of a mass concentration (g/L) representative of the entire production's magnetite suspension. When the sample dries, it is assumed that the magnetite is completely oxidized to maghemite. This assumption was used to convert the mass concentration to a molar concentration as described by Heathcock [3].

When the magnetite suspensions were stored over extended periods of time, the particles agglomerated [8]. To avoid conducting experiments with aggregated particles, prior to the initiation of any experiment, the stock suspension of magnetite was well mixed and the experimental aliquots of magnetite were briefly sonicated ($t < 1$ minute) to breakup aggregates and re-suspend the particles.

Oxidation Experiments. Prior to initiating an oxidation experiment, the magnetite particles were maintained under strictly anaerobic conditions. An oxidation experiment was started by transferring 250 mL of magnetite suspension to a three neck flask in the inert atmosphere of the glovebox. This flask was then sealed with rubber stoppers and removed from the glovebox. The anaerobic suspensions where shaken by hand and sonicated for approximately one minute to break up aggregates. The oxidation experimental setup was comprised of a three-neck flask, a glass diffuser rod, and a

condenser. House air was bubbled through the suspension using the air diffuser in the side stem of the flask, which rested on the bottom-center of the flask. The middle neck of the flask was occupied by the condenser, while the other two necks were sealed off with rubber stoppers. One of the rubber stoppers was penetrated by a stainless steel sampling tube and a thermocouple. The thermocouple was attached to a Cole-Palmer Temperature Controller that regulated the temperature of the system by controlling the Barnstead Electrothermal heating mantle on which the three neck flask rested. To insulate the system, the flask was wrapped in aluminum foil, helping maintain the desired temperature of the system. The setup is shown in Figure 3-1.

Experiments conducted for analysis by Raman spectroscopy employed a magnetite suspension of approximately 70 mM produced using NaOH. When sampling for Raman spectroscopy, the samples were withdrawn through the sampling tube into a syringe. Samples were withdrawn in approximately 4 mL aliquots which were more than sufficient for numerous Raman spectroscopy measurements. The magnetite samples withdrawn were immediately injected into anaerobic sealed glass vials and placed in an ice bath to quench the oxidation process. Samples were measured by Raman spectroscopy using a standard plastic grid from Fisher to retain the sample.

Oxidation experiments for dynamic light scattering (DLS) were conducted using a TMAOH synthesized magnetite at a concentration of approximately 2 mM. Oxidation and sampling was performed in the same manner as done for UV-Vis-NIR and Raman spectroscopy. A very small volume was needed for DLS analysis. Less than one milliliter was withdrawn for each time sample. Forty microliters of this sample was added to one milliliter of deionized water in a plastic disposable cuvette. This extremely

low concentration of magnetite minimizes particle to particle interactions which could cause aggregation during analysis.

Raman Spectrometer. The samples were analyzed by a Jobin Yvon Horiba Olympus BX41 Raman spectrometer. A red laser with wavelength of 632.8 nm was employed and spectral range measurements were obtained from 200 cm^{-1} to 1800 cm^{-1}. Three accumulations were run at acquisition times of 240 seconds each. The following parameters were also set: hole, 400 μm; slit, 150 μm; Spectro., 519.9 cm^{-1}, microscope objective, 10X; grating, 600. Under these conditions the Raman spot area is approximately 1 μm.

Dynamic Light Scattering. A Malvern Zetasizer 3000HS equipped with a helium/neon laser (γ = 633 nm). The refractive index employed was 1.59 and the temperature was held at 25 ^{o}C. Measurements were made in triplicates while the settings were set on the optimum position.

UV-VIS-NIR Spectrometer. Using a temperature controller, the temperature of the Cary 5000 UV-VIS-NIR spectrometer was set to the same temperature as the oxidation setup. Absorbance was measured over a spectral range of 400-1350 nm. Magnetite absorption begins in the near IR range of 800 nm to 2500 nm. At approximately 1400 nm the measurements are dominated by the background solution; therefore, the range was limited to 1350 nm. The entire range was measured in approximately 3 minutes by the spectrometer which was set to repeat the measurements for 20 minutes.

Arsenic Adsorption. Experiments conducted to investigate arsenic adsorption to magnetite were conducted by creating a stock solution of dissolved arsenic (III) oxide**.** A

basic medium was needed to dissolve the arsenic; therefore, a solution of 4 g/L sodium hydroxide was prepared [5]. Once the basic solution was added to the arsenic (III) oxide solid, the suspension was mixed vigorously until the arsenic was completely dissolved. The prepared stock solution was 20 mM As^{III}.

Using the stock arsenic solution, two separate experiments were conducted. One experiment was designed to analyze how the ionic strength of a magnetite/arsenic suspension affects adsorption, and another experiment for pH effects. Magnetite suspensions synthesized by NaOH were prepared within 60 mL glass vials and capped inside of the glovebox using aluminum caps with rubber septa. The experiments of ionic strength effects were conducted at pH ~8, adjusted with hydrochloric acid and sodium hydroxide, and the various ionic strengths were prepared with sodium chloride. The experiments of varying pH values were conducted at a sodium chloride concentration of 0.001 M. The various pH values were reached by the addition of hydrochloric acid and sodium hydroxide. Mass loadings of 0.026 g/L and 0.020 g/L magnetite were employed for investigations of ionic strength and pH respectively. Suspensions were buffered with 0.01 M HEPES. Before the addition of the arsenic to the magnetite suspensions, the sealed vials were placed on roll bars for continual 24 hour mixing. After the 24 hours of mixing, various arsenic volumes were spiked into the magnetite suspension in accordance with desired reactor arsenic concentrations. The spiked magnetite/arsenic suspensions were placed on roll bars for an additional 24 hours of continual mixing for maximum adsorption. Trials were done in triplicates as well as controls for each arsenic concentration which contained no magnetite.

Samples were prepared for inductively coupled plasma mass spectroscopy. The reactor vials were allowed sufficient time off of the roll bars before sampling for the magnetite to settle to the bottom. Ten milliliter samples, avoiding uptake of magnetite, were withdrawn from the reactor vials, to which, 200 microliters of concentrated nitric acid was added. By sampling supernatant that did not contain magnetite, the arsenic concentration reported by the ICP could be compared to the controls to observe arsenic removal by magnetite. Reactor vials that were presumed to present samples of arsenic concentrations higher than the ICP measurement ranges were diluted accordingly.

Inductively Coupled Plasma Mass Spectrometer. The mass spectrometer employed was an X-Series Thermo Electron Corporation Inductively Coupled Plasma Mass Spectrometer. The method followed was the Standard Method 3125-B.

Results and Discussion

Particle synthesis. Particles synthesized by the production method outlined in the Materials and Methods were characterized extensively by Heathcock. The method confidently produces nanoscale magnetite [3].

Oxidation. The oxidation setup (Figure 3-1) was successful for oxidizing magnetite. During the oxidation period, the dark black magnetite gradually changed to a red-brown color indicative of maghemite. Figure 3-2 shows the change in color due to oxidation.

Raman spectroscopy. To monitor magnetite oxidation, Raman spectroscopy was employed. The starting concentration of magnetite in these experiments was approximately 70 mM (mol Fe_3O_4/L) at pH 10. To induce rapid oxidation, the suspension's temperature was set at 80 ^oC and house gas (~21% oxygen) was bubbled

through the solution via a bubbling stone. As air is introduced to the suspension, the temperature drops; therefore, the rate was maximized but so as not to drop the temperature below the desired 80 ^{o}C. It is assumed that the rate was sufficient to assure that oxygen, the electron acceptor, was not the limiting factor in the oxidation process. Figure 4-1 indicates that at the initiation of oxidation, there was a single Raman band over the spectral range of 200-1800 cm^{-1} at approximately 671 cm^{-1}. The peak at 1640 cm^{-1} can be disregarded as it corresponds to water. As the oxidation time progressed, the intensity of this peak decreased. By the third hour of the oxidation period, this peak had disappeared. It was initially expected that as magnetite oxidized, the intensity of the peak would decrease, while a new peak at a different location would arise and intensify, indicating the increasing concentration of maghemite in the sample. The literature indicates that magnetite can be identified by a Raman band at approximately 667 cm^{-1}, while the band for maghemite is at approximately 670 cm^{-1} [1]. The observation that the Raman spectrometer measurements present a magnetite peak at a slightly different wavelength than expected is not significant as Raman bands tend to have reasonable fluctuation amongst spectrometers.

The Raman spectrometer was optimized to maximize magnetite identification. The data shows that the system was successful in monitoring the decreasing magnetite concentration within the sample; however, no new maghemite peak arose indicating the possibility that the system was not optimized for maghemite monitoring. It is likely that a longer acquisition time is required for the Raman spectrometer to measure maghemite. Additionally, the concentration of magnetite used for these Raman spectroscopic analyses is very high. It is possible that maghemite aggregated and settled to a level that the laser

was not able to illuminate. The laser used in Raman spectroscopy illuminates a specific volume of the sample, in which the contents of the illumination volume produce the Raman shifts, i.e. the intensity bands. The laser position was kept constant from sample to sample to assure that the same volume of sample was measured throughout the analysis. The laser does not have the capability to illuminate the entire sample so it is possible that concentrations were not the same from one illuminated sample to the next, especially if aggregation and settling occurred. Aggregation and settling could have occurred either during the Raman analysis which would result in false negative intensities, or during the oxidation trial which would result in lower concentrations being sampled.

It is interesting to note; however, a new peak visible at 498 cm^{-1} at 12 hours of oxidation. This peak corresponds with hematite. The peak was not present in any other sample so it is assumed that the concentration of hematite was not great enough until the twelfth hour to be detected. The hematite peak shows that the settings at which the Raman spectrometer were set were appropriate for hematite identification, as well as for magnetite identification. It is highly possible that if oxidation were allowed to continue past the twelfth hour, the hematite peak intensity would increase.

Dynamic Light Scattering. Figure 4-2 presents data obtained from dynamic light scattering (DLS) showing that over the time period of oxidation at 60 ^{o}C, 70 ^{o}C, and 80 ^{o}C the particles did not aggregate significantly as oxidation proceeded. The lack of significant aggregation over time leads to the belief that there was not much settling over the hours of oxidation within the oxidation setup. The particles used were synthesized by TMAOH and oxidized at a concentration of 2 mM. As characterized by Tang et al. and

Heathcock, all synthesized particle are assumed to be less than 10 nm in diameter [5, 9]. However, the trials began with fairly aggregated particles. The data shows that the aggregate size did not change significantly throughout oxidation.

The different temperatures show dissimilar aggregate sizes. At the initiation of oxidation (t=0), all the sample temperatures were the same, yet they all show different aggregate sizes. Immediately before beginning the experiments, the samples were sonicated for approximately one minute. The different sizes between the trials only show that the sonication was not uniform between the trials. After the first sample, the desired temperatures were reached and it appears that significant further aggregation did not occur. At 80 ^{o}C, the aggregate size increased 36% from 697 nm to 948 nm in 3 hours of oxidation. At 70 ^{o}C, the aggregate size increased almost 60%, from 324 nm to 515 nm in 6 hours of oxidation. The aggregate size at oxidation initiation for 60 ^{o}C was 429 nm. After one of our oxidation the aggregate size increased almost 200% to 1290 nm. By the tenth hour of oxidation, the aggregate size only changed by another 0.5% to 1283 nm. It can be assumed that the initial aggregation size at 60 ^{o}C was an anomaly based on the trends of the other temperatures and the trend of 60^{o}C after the first hour. It is assumed that the increases in aggregation over time are insignificant since the aggregates were initially large. It is difficult to make generalizations of the aggregation relationship to oxidation with only the data presented. The particles used for DLS analysis were representative of the particles used for UV-Vis-NIR spectroscopy analysis; however, the particles had been stored for a much longer time and; therefore, extensive aggregation occurred.

UV-Vis-NIR Spectroscopy. UV-Vis-NIR spectroscopy work was conducted using particles synthesized in NaOH. The methods followed were the same as those described in Chapter III. Figure 4-3 presents the absorption spectrum of the magnetite oxidation at 80 ^{o}C. It is shown that using NaOH synthesized particles for UV-Vis-NIR analysis produces inconsistent data. The vast changes in absorption in the UV-region of the spectrum suggest aggregation within the oxidation setup. Aggregation within the setup results in lower concentrations sampled and analyzed. The lower concentrations produce lower absorbencies which are not representative of earlier sample concentrations. Chapter III presented analysis of particles synthesized in the stabilizer, TMAOH. The TMAOH particles produced reliable oxidation absorption data due to a more stable suspension. The NaOH particles were not able to be analyzed due to great aggregation effects on absorption.

Arsenic Adsorption. The goal of the preliminary work done to investigate arsenic adsorption to magnetite was to observe adsorption changes due to various pH values and various ionic strengths.

Effect of ionic strength. Figure 4-3 depicts how arsenic adsorption is affected by ionic strength. By increasing ionic strength of a magnetite suspension it is assumed that aggregation of the particles should increase by compressing the electric double layer [3]. Thicker electric double layers help to maintain suspension stability. As the particles become closer to one another due to the compression, the particles begin to agglomerate by van der Waal forces [1]. Yean et al. has shown that an increase in surface area (m^2/g) will increase arsenic adsorption. An increase in aggregation decreases available surface area for arsenic complexes. The figure shows various interesting things

for further investigation. The figure shows that the lowest ionic strength tested has the highest adsorption capabilities as arsenic concentrations within the suspension increase, as expected. The lowest ionic strength solution should have the least aggregation and; therefore, the most available surface area. There appears to be a steady increase in adsorption of arsenic as the arsenic concentration increases. At the highest arsenic concentration within the suspensions, 500 μM As^{III}, neither the 0.001 M NaCl nor 0.01 M NaCl suspensions have seemed to have reached their maximum adsorption capabilities. A maximum adsorption would have been marked by a constant value of arsenic adsorbed per mass of magnetite (μmol/g) as the arsenic concentration within the suspension increases; a horizontal line. The lack of a plateau restrains the possibility of calculating an accurate Langmuir isotherm. Further increasing arsenic concentrations are necessary to present maximum arsenic adsorption capabilities for a given mass loading of magnetite. As arsenic concentrations increase, the percent of removal decreases. At 0.001 M NaCl and the lowest concentration of arsenic, 10 μM, the magnetite was able to remove 16.2% of the arsenic by adsorption. At the same ionic strength but the highest concentration of arsenic, 500 μM, the magnetite adsorbed 5.2% of the arsenic. The magnetite at an ionic strength of 0.01 M NaCl showed very similar results; 16.8% removal at the lower arsenic concentration and 4.3% removal at the highest arsenic concentration.

The highest ionic strength shows a different trend. The adsorption of arsenic increased as arsenic concentrations increased, just as in the lower ionic strength solutions. It does appear; however; that adsorption was higher at 0.1 M NaCl at lower arsenic concentrations than for the lower ionic strengths, which was unexpected as it was

expected that aggregation should be greater at the higher ionic strength. At approximately 100 μM arsenic, there was a dramatic decrease in absorption that continued as arsenic concentrations increased. At the lowest concentration of arsenic the magnetite in a 0.1 M NaCl suspension was able to remove 34% of the arsenic. However, at the highest arsenic concentration, 500 μM arsenic, the removal was less than 1%. The arsenic speciation should be dominated by the neutral species, $H_3AsO_3^0$, which would not increase the ionic strength of the suspension significantly even as arsenic concentrations increased. It appears that as arsenic concentrations increased, adsorption increased until the arsenic concentration induced significant aggregation, greatly decreasing adsorption. It had been hypothesized previously that high ionic strength would negatively affect adsorption; however, at low arsenic concentrations, high ionic strength seemed to increase adsorption. It was not until high arsenic concentrations that a negative effect of ionic strength was seen. Further investigations will need to be done to investigate this trend.

Effect of pH. The pK_a for As^{III} is 9.2. As pH values approach this pK_a value, the neutral species that binds to magnetite $H_3AsO_3^0$, increases in concentration. It is assumed that as the pH increases towards the pK_a, the adsorption should increase as more arsenic should be present as the neutral binding species. At higher pH values, the suspension should be more stable as the surface of the magnetite should be more negative, increasing repulsive forces between magnetite particles which will inhibit aggregation [1]. Studies have shown that As^{III} adsorption increases with increasing pH [6]. Figure 4-4 shows the results of testing arsenic adsorption at different pH values. It does not show the expected trends. At lower arsenic concentrations, the highest pH value

tested, pH 9, shows very similar adsorption capabilities as the other pH values. At the second to highest arsenic concentration, 300 μM, pH 9 has the highest adsorption, which then decreases as arsenic concentration increases to 500 μM. It is at this high arsenic concentration that the magnetite adsorbs a substantial amount more arsenic at lower pH values than at pH 9. The other pH values show major adsorption increases at the high arsenic concentrations. The trend that was seen, but not expected, was that as pH decreased, adsorption increased. The lowest pH value, pH 7, had the highest adsorption at the highest arsenic concentration. At the lowest arsenic concentration, the magnetite was able to remove 12.4% at pH 9 which increased gradually to 16.4% removal as pH decreased to pH 7. At the highest concentration of arsenic, the magnetite removed 3% at pH 9 which increased to 9% at pH 7.

Conclusions.

Chapter IV presented preliminary work for oxidation monitoring and arsenic adsorption. From this work it can be seen that it is difficult to detect maghemite while at the same time monitoring magnetite concentration changes within a sample using Raman spectroscopy. In the final sample of oxidation, a hematite peak was seen. Using Raman spectroscopy, monitoring the decreasing magnetite concentration was more successful than monitoring the maghemite concentration which was never detected by the Raman spectrometer.

Particles synthesized in TMAOH were oxidized and their aggregate size measured using dynamic light scattering. All of the temperature trials of oxidation showed insignificant aggregation. The individual particle size was characterized by Tang et al. to be less than 10 nm; however, very large aggregates were present at the initiation of

oxidation. The slight growth of the already large aggregates was considered to be insignificant.

Particles oxidized that were produced in NaOH showed erratic absorptions in the UV-region of the absorption spectra making analysis impossible of these types of particles.

The arsenic adsorption effects due to ionic strength show something rather interesting, but require more exploration to be explained. Adsorption seemed to be increased at the highest ionic strength but then rapidly decreased past a certain maximum arsenic concentration. The pH effects were the opposite of what was expected. It was seen that as pH decreased the adsorption increased. Due to the lack of further investigation of arsenic adsorption, these trends cannot be fully explained.

References

1. R.M. Cornell, U.S., *The Iron Oxides Structure, Properties, Reactions, Occurrences and Uses*. Second ed. 2003: Wiley-VCH Verlag GmbH & Co. KGaA, Weinheim. 664.
2. Yavuz, C.T., et al., *Low-field magnetic separation of monodisperse Fe3O4 nanocrystals.* Science, 2006. **314**(5801): p. 964-967.
3. Vikesland, P.J., et al., *Particle size and aggregation effects on magnetite reactivity toward carbon tetrachloride.* Environmental Science & Technology, 2007. **41**(15): p. 5277-5283.
4. Shebanova, O.N. and P. Lazor, *Raman study of magnetite (Fe3O4): laser-induced thermal effects and oxidation.* Journal of Raman Spectroscopy, 2003. **34**(11): p. 845-852.
5. Tang, J., et al., *Magnetite Fe3O4 nanocrystals: Spectroscopic observation of aqueous oxidation kinetics.* Journal of Physical Chemistry B, 2003. **107**(30): p. 7501-7506.
6. Yean, S., et al., *Effect of magnetite particle size on adsorption and desorption of arsenite and arsenate.* Journal of Materials Research, 2005. **20**(12): p. 3255-3264.
7. Yu, W.W., et al., *Aqueous dispersion of monodisperse magnetic iron oxide nanocrystals through phase transfer.* Nanotechnology, 2006. **17**(17): p. 4483-4487.
8. Vayssieres, L., et al., *Size tailoring of magnetite particles formed by aqueous precipitation: An example of thermodynamic stability of nanometric oxide particles.* Journal of Colloid and Interface Science, 1998. **205**(2): p. 205-212.
9. Heathcock, A.M., *Characterization of Magnetite Nanoparticle Reactivity in the Presence of Carbon Tetrachloride*, in *Civil and Environmental Engineering*. 2006, Virginia Polytechnic and State University: Blacksburg. p. 50.

Tables and Figures

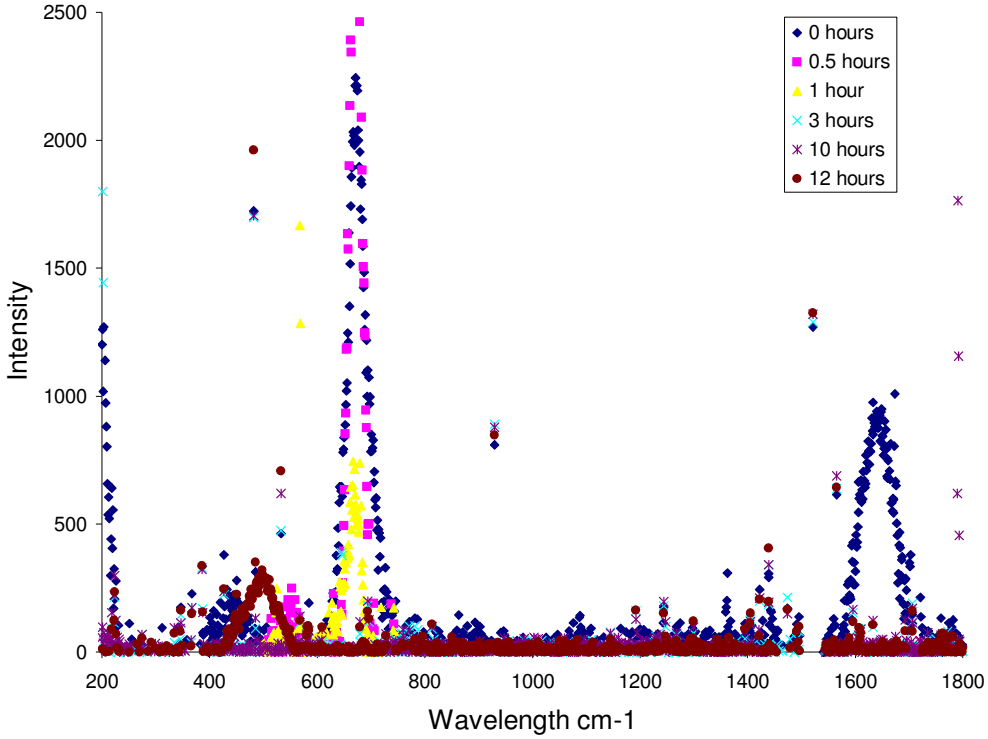

Figure 4-1. Raman spectroscopy spectra of magnetite oxidation at 80 ^{o}C.

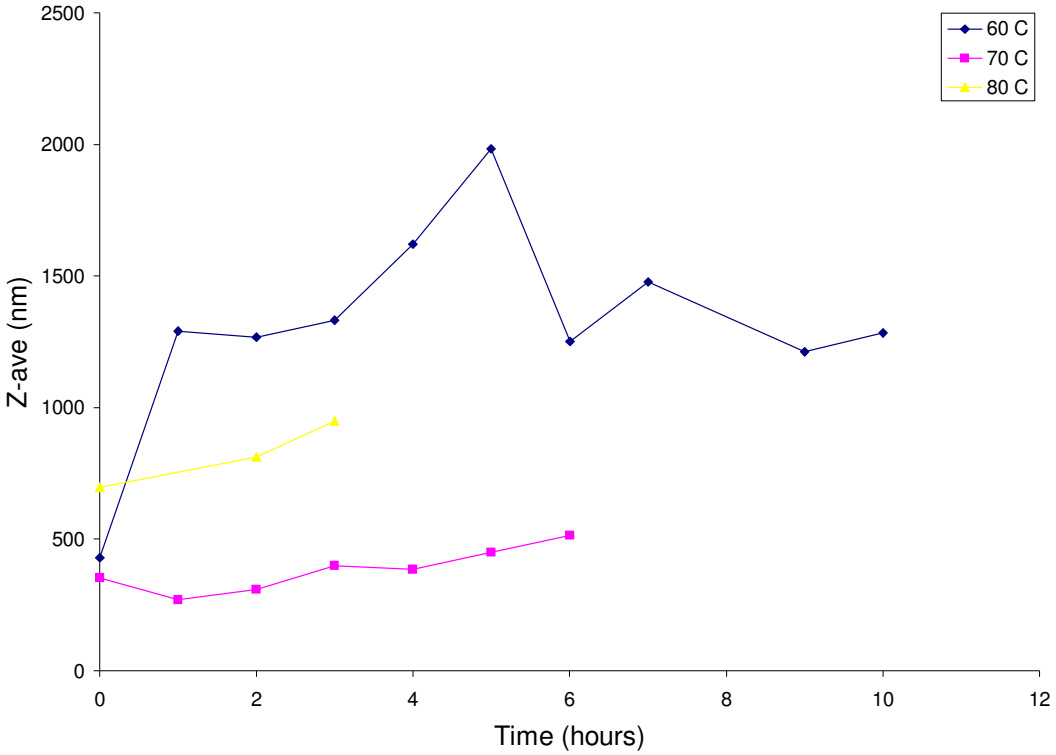

Figure 4-2. Dynamic light scattering over the oxidation period at 2 mM (mol Fe_3O_4/L). Points are averages of three measurements and the line shows the possible trend between points.

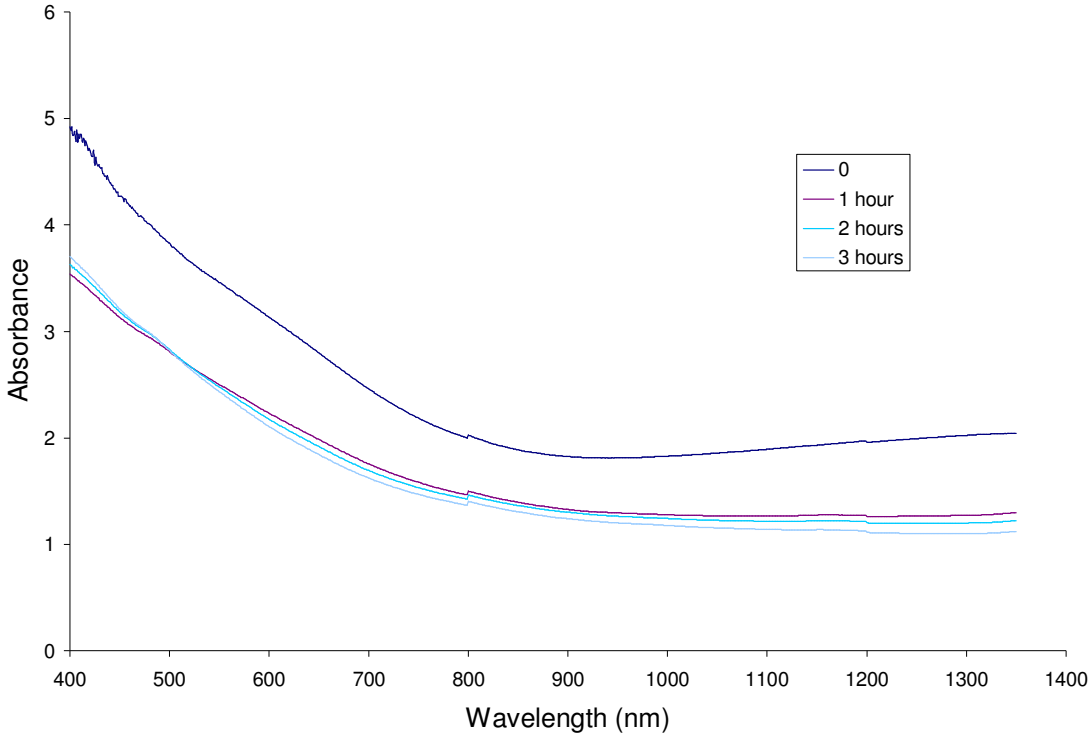

Figure 4-3. Oxidation of magnetite particles synthesized with NaOH at 80 ^{o}C.

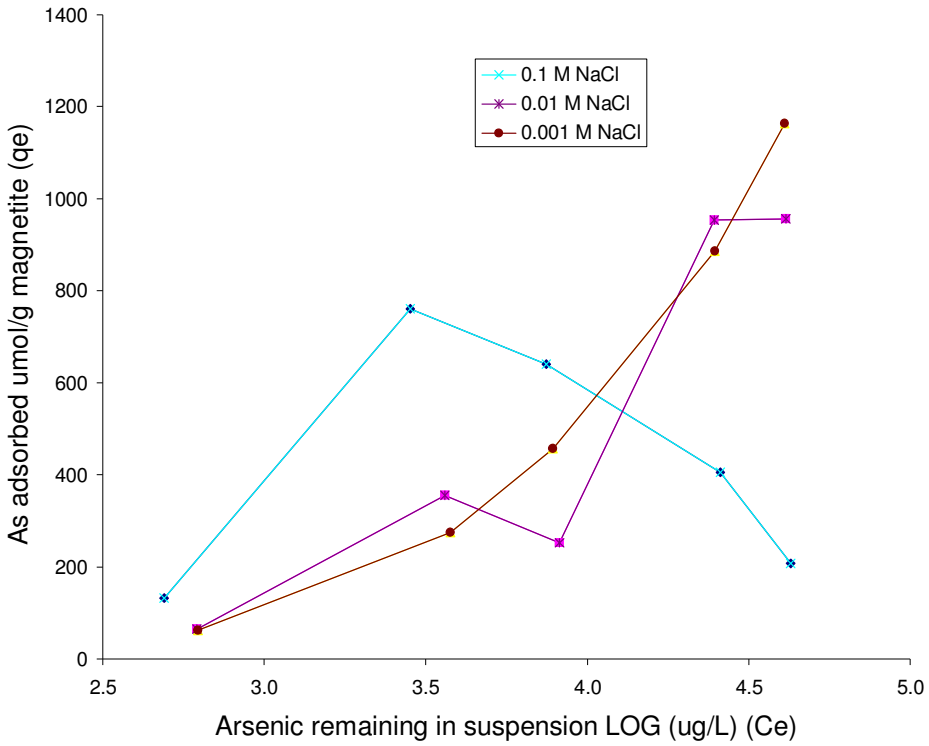

Figure 4-4. Arsenic adsorption to magnetite at various sodium chloride concentrations.

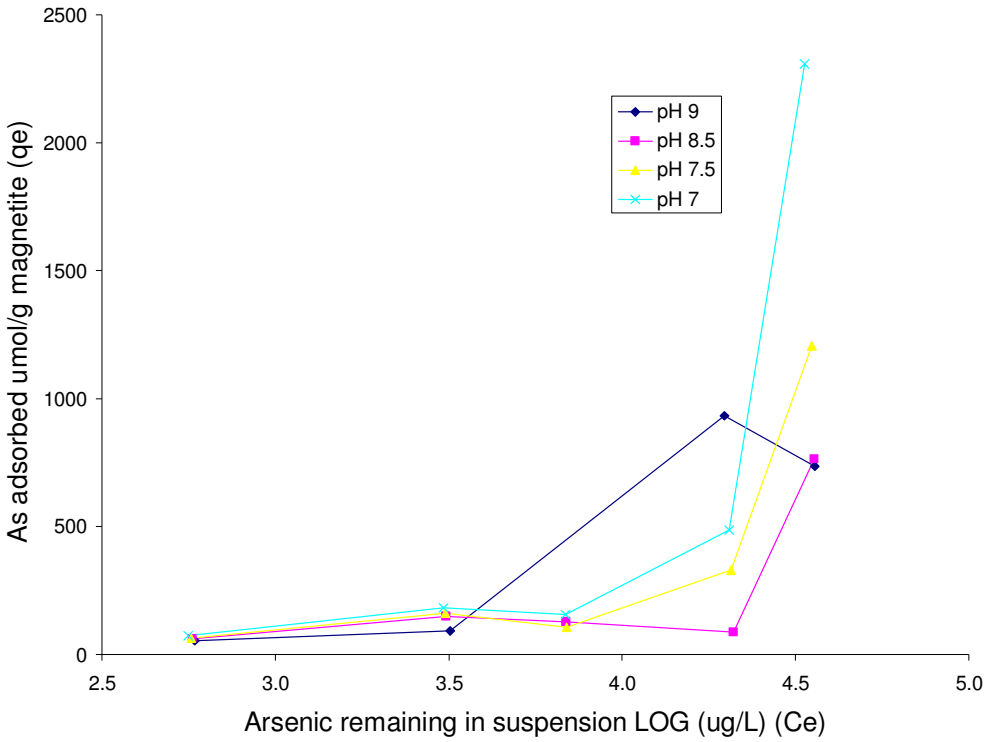

Figure 4-5. Arsenic adsorption at various pH values.

V. Engineering Significance

Many past studies have acknowledged iron oxides' capabilities of environmental remediation [1-5]. Magnetite's magnetic properties and ability to adsorb contaminants such as arsenic and reduce chlorinated compounds persuade the engineering field to further investigate the use of magnetite for *in situ* remediation [5, 6]. When magnetite is involved in remediation such as oxidation/reduction of carbon tetrachloride, the magnetite is transformed into a different iron oxide, maghemite. This study investigated and monitored magnetite transformation to maghemite by UV-Vis-NIR analysis. By controlling oxidation through temperature control, oxidation characteristics were developed. The transformations that magnetite underwent in this study, with oxygen as the oxidant, are the same transformations that magnetite undergoes during the reduction of chlorinated hydrocarbons. As magnetite transforms to maghemite, the properties and remediation capabilities change accordingly. Being able to monitor and understand the oxidation process of magnetite will aid engineers in understanding how magnetite and its oxidant interact as transformation proceeds through oxidation/reduction.

This study has also improved the understanding of the UV-Vis-NIR spectrometer. It has shown that different types of transitions within an iron oxide respond uniquely at different temperatures effecting the measurements of transformation. Only by understanding what transitions are occurring during spectroscopy analysis and their dependence on temperature can an accurate interpretation be made. The study has improved the understanding of the relationship between the UV-Vis-NIR spectrometer, temperature, and the transitions of magnetite and maghemite, which will improve how future studies interpret data involving the same components.

References

1. R.M. Cornell, U.S., *The Iron Oxides Structure, Properties, Reactions, Occurrences and Uses*. Second ed. 2003: Wiley-VCH Verlag GmbH & Co. KGaA, Weinheim. 664.
2. Heathcock, A.M., *Characterization of Magnetite Nanoparticle Reactivity in the Presence of Carbon Tetrachloride*, in *Civil and Environmental Engineering*. 2006, Virginia Polytechnic and State University: Blacksburg. p. 50.
3. Vikesland, P.J., et al., *Particle size and aggregation effects on magnetite reactivity toward carbon tetrachloride.* Environmental Science & Technology, 2007. **41**(15): p. 5277-5283.
4. McCormick, M.L., E.J. Bouwer, and P. Adriaens, *Carbon tetrachloride transformation in a model iron-reducing culture: Relative kinetics of biotic and abiotic reactions.* Environmental Science & Technology, 2002. **36**(3): p. 403-410.
5. Yean, S., et al., *Effect of magnetite particle size on adsorption and desorption of arsenite and arsenate.* Journal of Materials Research, 2005. **20**(12): p. 3255-3264.
6. Yavuz, C.T., et al., *Low-field magnetic separation of monodisperse Fe3O4 nanocrystals.* Science, 2006. **314**(5801): p. 964-967.

VI. Conclusions

The following presents the conclusions drawn from the study:

- The oxidation of nanoscale magnetite produces a decreasing absorption band in the NIR-region of the UV-Vis-NIR spectrum, while producing an increasing absorption band in the UV-region of the spectrum.
- The temperature at which samples are measured within the spectrometer effect the transitions differently.
- The magnetically coupled Fe^{III}-Fe^{III} transitions are greatly affected by measurement temperatures. Higher temperatures tend to dampen the absorption of the Fe^{III} transitions, while lower temperatures tend to amplify the absorption.
- The Fe^{II}-Fe^{III} electron hopping transition shows a slightly higher absorption at higher measurement temperatures and slightly decreases at lower temperatures.
- At lower temperatures the isosbestic point, which is the wavelength at which the Fe^{III}-Fe^{III} and Fe^{II}-Fe^{III} transition absorptions are equal, shifts towards longer wavelengths due to the increased absorption of the Fe^{III}-Fe^{III} transitions.
- The rate at which magnetite is oxidized greatly increases with increasing temperature.
- Diffusion coefficients generated by UV-Vis-NIR data does not correlate to the same equations that calculate diffusion coefficients from Fe^{II} diffusion data.

Appendix A

The data analysis of temperature effect on absorption at 1260 nm and 450 nm presented in Figure 3-7.

1260 nm

SUMMARY OUTPUT

Regression Statistics	
Multiple R	0.980935466
R Square	0.962234389
Adjusted R Square	0.924468777
Standard Error	0.00366044
Observations	3

ANOVA

	Df	*SS*	*MS*	*F*	*Significance F*
Regression	1	0.00034139	0.00034139	25.47911596	0.124508961
Residual	1	1.33988E-05	1.33988E-05		
Total	2	0.000354789			

	Coefficients	*Standard Error*	*t Stat*	*P-value*	*Lower 95%*	*Upper 95%*	*Lower 95.0%*	*Upper 95.0%*
Intercept	1.771163974	0.08876689	19.95297998	0.031879326	0.643273699	2.899054248	0.643273699	2.899054248
X Variable 1	-153.556409	30.42115995	-5.047684217	0.124508961	-540.0938956	232.9810776	-540.0938956	232.9810776

450 nm

SUMMARY OUTPUT

Regression Statistics	
Multiple R	0.962579022
R Square	0.926558374
Adjusted R Square	0.853116747
Standard Error	0.19225057
Observations	3

ANOVA

	Df	*SS*	*MS*	*F*	*Significance F*
Regression	1	0.466300385	0.4663	12.61625622	0.174709446
Residual	1	0.036960282	0.03696		
Total	2	0.503260667			

	Coefficients	*Standard Error*	*t Stat*	*P-value*	*Lower 95%*	*Upper 95%*	*Lower 95.0%*	*Upper 95.0%*
Intercept	-12.3655997	4.662139841	-2.65234	0.22952995	-71.60370301	46.87250361	-71.60370301	46.87250361
X Variable 1	5675.123445	1597.754548	3.551937	0.174709446	-14626.27296	25976.51985	-14626.27296	25976.51985

Appendix B

The following is a list of the figures and the file name in which the raw data can be found.

Tables

Table 3-1. Absorption summary for all temperatures-TMAOH (60, 70, 80) Run 2.xls

Table 3-2. Diffusion Coefficients oxidation of magnetite-TMAOH 80 constant all runs.xls, Runs.xls

Figures

Figure 3-4. First and second scans at initiation (t=0) of oxidation-TMAOH (60, 70, 80) all runs.xls

Figure 3-5. Figure 3-5. The change in absorption through the measurement period at t = 0-AbsvsAbs all runs averaged.xls, TMAOH (60, 70, 80) constant all runs.xls

Figure 3-6. The effect of temperature on the first and second scan absorptions-TMAOH (60, 70, 80) Run 2.xls

Figure 3-7. The effect of temperature on the transitions-TMAOH 80 all runs.xls

Figure 3-8. a) Oxidation of magnetite at 60 ^{o}C measured by UV-VIS-NIR spectroscopy-TMAOH 60 C constant all runs.xls

Figure 3-9. a) Oxidation of magnetite at 70 ^{o}C measured by UV-VIS-NIR spectroscopy-TMAOH 70 C constant all runs.xls

Figure 3-10. a) Oxidation of magnetite at 80 ^{o}C measured by UV-VIS-NIR spectroscopy-TMAOH 80 constant all runs.xls

Figure 3-11. The effect of sequential scans on absorption at 1260 nm-AbsvsAbs all runs averaged.xls

Figure 3-12. The effect of different scans on the kinetics of oxidation-all together.xls

Figure 3-14. Beer's Law related to the change in absorption at 1260 nm and 450 nm-TMAOH 80 constant all runs.xls

Figure 3-15. The effect of sequential scans on absorption within the same sample at a measuring temperature of 25^{o}C-TMAOH (60, 80) C not constant Temp.xls

Figure 3-16. UV-Vis-NIR spectroscopy analysis with temperature measurements set at 25^{o}C- TMAOH (60, 80) C not constant Temp.xls

Figure 3-17. a) Oxidation of magnetite using the second scan from the measuring period at 60 ^{o}C by UV-VIS-NIR spectroscopy-TMAOH 60 C constant Run 2.xls

Figure 3-18. a) Oxidation of magnetite using the second scan from the measuring period at 70 ^{o}C by UV-VIS-NIR spectroscopy- TMAOH 70 C constant Run 2.xls

Figure 3-19. a) Oxidation of magnetite using the second scan from the measuring period at 80 ^{o}C by UV-VIS-NIR spectroscopy- TMAOH 80 C constant Run 2.xls

Figure 3-20. The absorption at 1260 nm-TMAOH 80 constant all runs.xls

Figure 3-21. The absorption at 450 nm-TMAOH 80 constant all runs.xls

Figure 3-22. $\frac{Absorbance_{1260nmt=x}}{Absorbance_{1260nm\infty}} \times \frac{1}{t}$ versus $\frac{1}{t^{1/2}}$ plot **-**TMAOH 80 constant all runs.xls

Figure 4-1. Raman spectroscopy spectra of magnetite oxidation at 80 ^{o}C-best oxidation.xls

Figure 4-2. Dynamic light scattering over the oxidation-DLS.xls

Figure 4-3. Oxidation of magnetite particles synthesized with NaOH at 80 ^{o}C- Regular magnetite UV-vis.xls

Figure 4-4. Arsenic adsorption to magnetite at various sodium chloride concentrations-Arsenic 3 different salt concentrations.xls

Figure 4-5. Arsenic adsorption at various pH values-Arsenic different pH levels.xls